Available online at www.sciencedirect.com

SCIENCE DIRECT®

Sedimentary Geology 179 (2005) 5–29

Sedimentary Geology

www.elsevier.com/locate/sedgeo

Density- and viscosity-stratified gravity currents: Insight from laboratory experiments and implications for submarine flow deposits

L.A. Amy [a,b,*], J. Peakall [b], P.J. Talling [a]

[a] *Centre for Environmental and Geophysical flows, Department of Earth Sciences, University of Bristol, Bristol, BS8 1RJ, UK*
[b] *Earth and Biosphere Institute School of Earth and Environment, University of Leeds, Leeds, LS2 9JT, UK*

Received 22 April 2004; accepted 6 April 2005

Abstract

Vertical stratification of particle concentration is a common if not ubiquitous feature of submarine particulate gravity flows. To investigate the control of stratification on current behaviour, analogue stratified flows were studied using laboratory experiments. Stratified density currents were generated by releasing two-layer glycerol solutions into a tank of water. Flows were sustained for periods of tens of seconds and their velocity and concentration measured. In a set of experiments the strength of the initial density and viscosity stratification was increased by progressively varying the lower-layer concentration, C_L. Two types of current were observed indicating two regimes of behaviour. Currents with a faster-moving high-concentration basal region that outran the upper layer were produced if $C_L < 75\%$. Above this critical value of C_L, currents were formed with a relatively slow, high-concentration base that lagged behind the flow front. The observed transition in behaviour is interpreted to indicate a change from inertia- to viscosity-dominated flow with increasing concentration. The reduction in lower-layer velocity at high concentrations is explained by enhanced drag at low Reynolds numbers. Results show that vertical stratification produces longitudinal stratification in the currents. Furthermore, different vertical and temporal velocity and concentration profiles characterise the observed flow types. Implications for the deposit character of particle-laden currents are discussed and illustrated using examples from ancient turbidite systems.

Keywords: Sediment gravity flows; Turbidity currents; Subaqueous debris flows; Flow stratification; Analogue experiments

1. Introduction

Sediment-laden density flows with a wide range of sediment concentrations occur in subaqueous environments (Mulder and Alexander, 2001). These density flows include turbidity currents and debris flows.

* Corresponding author. Centre for Environmental and Geophysical flows, Department of Earth Sciences, University of Bristol, Bristol, BS8 1RJ, UK. Tel.: +44 117 954 5235; fax: +44 117 925 3385.
E-mail address: l.amy@bristol.ac.uk (L.A. Amy).

0037-0738/$ - see front matter © 2005 Elsevier B.V. All rights reserved.
doi:10.1016/j.sedgeo.2005.04.009

Collectively they dominate sediment flux from shallow to deep marine environments in many locations (Kneller and Buckee, 2000), and form some of the most voluminous sediment accumulations on Earth (Bouma et al., 1985). Individual events may transport tens, or even hundreds, of cubic kilometres of sediment (Piper et al., 1999; Wynn et al., 2002). Ancient deposits of sedimentary density flows form many of the world's largest petroleum reservoirs (Weimer and Link, 1991), whilst modern flow events are a significant hazard to seafloor structures (Barley, 1999).

Almost all particulate gravity flows contain vertical gradients in suspended-sediment concentration where particle concentration decreases upwards away from the bed (Fig. 1). Particle stratification is a property of laboratory currents (e.g., Middleton, 1966; Postma et al., 1988), numerical simulations (e.g., Stacey and Bowen, 1988; Felix, 2002), and is recorded in the few natural flows that have been instrumented (e.g., Normark, 1989; Chikita, 1990). This characteristic develops within flows carrying a range of grain sizes since it takes more energy to suspend relatively dense and large particles at a point above the bed. Stratification may become more pronounced due to variable rates of particle settling, mixing with ambient fluid and entrainment of substrate material (Fisher, 1995; Peakall et al., 2000; Gladstone et al., 2004). Since both the density and viscosity of particle–fluid mixtures are governed by particle concentration, flows are also vertically stratified in terms of these properties.

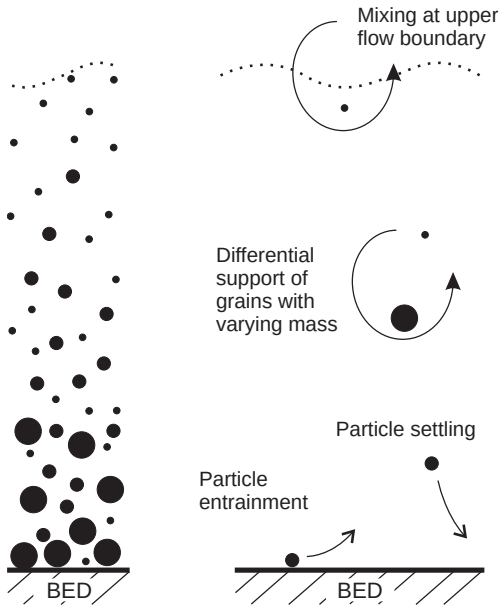

Fig. 1. Schematic diagram showing particle stratification that occurs within sediment gravity flows and its principal causes.

There is strong evidence for stratification in particulate density currents, however, few studies have investigated in a systematic manner how density and viscosity stratification influence flow behaviour. Gladstone et al. (2004) investigated the behaviour of two-layer, lock-exchange, stratified density flows using laboratory experiments. They demonstrated that layer density and volume have a marked effect on the current's evolution and the resulting flow structure. Their results are applicable to inertial, surge-type density-stratified currents. In this study experiments were run to investigate currents that were viscosity-stratified and density-stratified with relatively long durations. These experimental currents should be more representative of natural particle-laden currents with relatively large volumes and high particle concentration (Peakall et al., 2001). A series of experiments is presented in which the initial density and viscosity stratification of solute-driven currents was systematically varied. In these experiments the velocity and concentration structure of flows were recorded using instrumentation. The interaction between layers was also analysed from recorded video footage. These experiments allow the role of density and viscosity stratification on the behaviour of the flow to be assessed. Implications for sediment deposition from particle-laden currents and resulting deposit character are discussed.

2. Flow stratification

This paper presents new data on the concentration distributions of density currents. Existing data on the stratification of sediment gravity flows has been reviewed by Peakall et al. (2000) and Kneller and Buckee (2000). Laboratory studies have shown that different types of flow stratification can occur depending on flow concentration. Relatively low concentration (<10% by volume) and fully turbulent, depositional currents display broadly continuous profiles with concentration decreasing gradually up-

wards (Fig. 2A–C). A gradual concentration profile occurs under both subcritical and supercritical flow conditions. Grain-size classes are distributed differently throughout the flow depth (García, 1994). Finer particles tend to be more evenly distributed throughout the flow depth compared to coarser grains. Numerical models (Stacey and Bowen, 1988; Felix, 2002) and measurements of natural turbidity currents (Normark, 1989; Chikita, 1990) also suggest continuous profiles for relatively low-concentration currents that are weakly depositional.

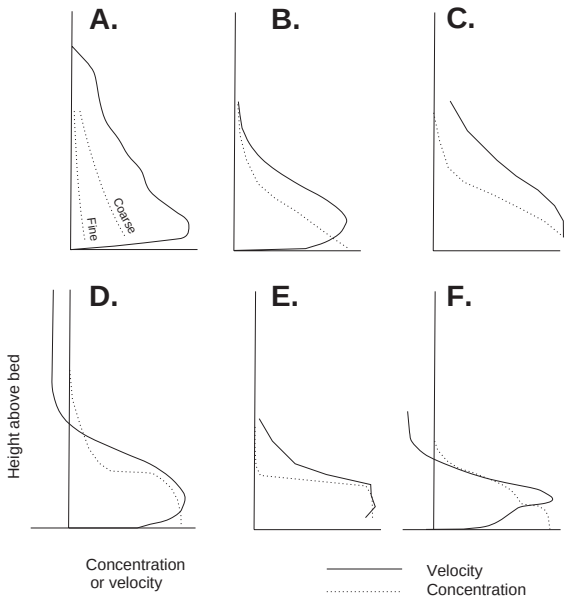

Fig. 2. Measured concentration and velocity profiles of laboratory sediment gravity flows. The vertical dimension is normalised with respect to the height of the velocity maximum and the horizontal scale is normalised using the velocity and concentration maxima. (A) Continuous concentration profile; strongly depositional subcritical turbidity current (García, 1994). The distributions of fine (5 μm) and coarse (32 μm) grain size fractions are also shown. (B) Nearly continuous concentration profile (slight inflexion above the velocity maximum); weakly depositional subcritical turbidity current on a low-angle slope (Altinakar et al., 1996). (C) Nearly continuous concentration profile; low-concentration (1055 kg m^{-3}) fluid mudflow (van Kessel and Kranenburg, 1996). (D) Two-layer model with a stepped concentration profile above the velocity maximum, based on visual observations of strongly depositional lock release turbidity currents (Middleton, 1966, 1993). (E) Stepped concentration and velocity profile; high-concentration (1200 kg m^{-3}) fluid mudflow (van Kessel and Kranenburg, 1996). (F) Multi-stepped concentration profile inferred from video and modified velocity profile measured using trajectories of moving particles; high-concentration turbidity current with starting concentration of 35–40% volume fraction (Postma et al., 1988).

Few measurements of the concentration profiles of high-concentration, particulate laboratory currents exist (>20% by volume). Based on visual observations of strongly depositional currents, Middleton (1966, 1993) proposed a two-layer model. This model suggests a stepped profile with a high-concentration lower layer overlain by a more dilute and relatively turbulent upper layer, also observed in other experiments (e.g., Hampton, 1972; Mohrig et al., 1998; Hallworth and Huppert, 1988; Marr et al., 2001). A study by van Kessel and Kranenburg (1996) measured the concentration profiles of fluid mudflows and demonstrated a stepped profile for those with relatively high concentrations. More importantly, in a set of experiments, they were able to document a change from a gradual (Fig. 2C) to a stepped profile (Fig. 2E) with increasing mud concentration and were able to show that this occurred in conjunction with a transition from turbulent to laminar flow. In another experimental study on a high-concentration flow, using cohesionless sediment, a laminar-moving high-concentration basal layer was observed to form (Postma et al., 1988). This took the form of a wedge propagating behind the head of the current and below an overriding turbulent, but strongly stratified, upper region. The inferred velocity and concentration profile in these currents is slightly different to those of high-concentration fluid mudflows (Fig. 2F). The velocity profile has an ‘overhanging nose’ with a discrete reduction in values below the velocity maximum, whilst the concentration profile has two steps one below and one above the velocity maximum. However, these measurements were estimated somewhat crudely compared to the other reported studies, because flow velocity was derived from the motion of particles adjacent to the tank wall captured by film, and thus do not exclude wall affects, whilst concentration was estimated visually.

3. Experimental method

The experiments were run in a glass-walled, gravity-current tank located in the School of Earth and Environment, University of Leeds. The tank was 6 m

in length, 0.5 m in width and was filled with water to a depth of ~1.5 m (Fig. 3). Stratified flows were generated using two aqueous solutions with different concentrations of glycerol. Each solution was first mixed in an external reservoir tank and circulated from this tank into a header box and back again via an overflow system. Solutions were dyed different colours and seeded with small amounts ($\ll$1% by volume) of millimetre-sized neutrally buoyant particles to aid flow visualisation. A small amount of silica flour (grain size <50 μm diameter) was also added to help flow velocity measurement (see below). Experiments were started by opening a valve on the header boxes and allowing the solutions to gravity drain into the main tank. The discharge rate from each header box was kept constant by maintaining a constant fluid head in the header box. It was not possible, however, to keep the discharge rate the same for solutions of different glycerol concentrations. The discharge rate varied for fluids of different glycerol concentrations (i.e., between different layers and experiments) from 2–4 l/s owing to their different fluid densities and viscosities. The solutions passed through an inlet box which was laid flat on the tank floor. The inlet box partitioned the two glycerol solutions into a vertically stratified release, with a lower relatively dense layer and an upper less-dense layer. It also dampened the initial turbulence by passing the fluid through a section filled with polystyrene chips. Currents flowed down a 3.5-m-long, smooth, floor inclined at 3°. Fluid at the end of the tank was collected in a sump and pumped out of the tank to minimise the effects of flow reflection and changes in the ambient fluid depth.

3.1. Solute properties

In these experiments solutions were used instead of particle–water slurries. This approach was chosen since it was technically difficult to generate high-concentration currents with long durations and with controlled initial stratifications using sediment. Solutions of aqueous glycerol were chosen since they have similarities in their density and viscosity with sediment–water mixtures. Glycerol ($C_3H_8O_3$) has a density of 1260 kg m^{-3} and viscosity of ~1.5 kg m^{-1} s^{-1} at 20 °C (CRC Handbook of Chemistry and Physics). For aqueous glycerol solutions viscosity increases by several orders of magnitude with increasing glycerol concentrations from ~10^{-3} to 1.5 kg m^{-1} s^{-1} (Fig. 4). The viscosity of sediment–water mixtures also increases strongly by several orders of magnitude at particle concentrations greater than 40–50% for mixtures composed of cohesionless particles (Richardson and Zaki, 1954; Kreiger and Dougherty, 1959), and at relatively low particle concentrations for those containing cohesive particles (Major and Pierson, 1992;

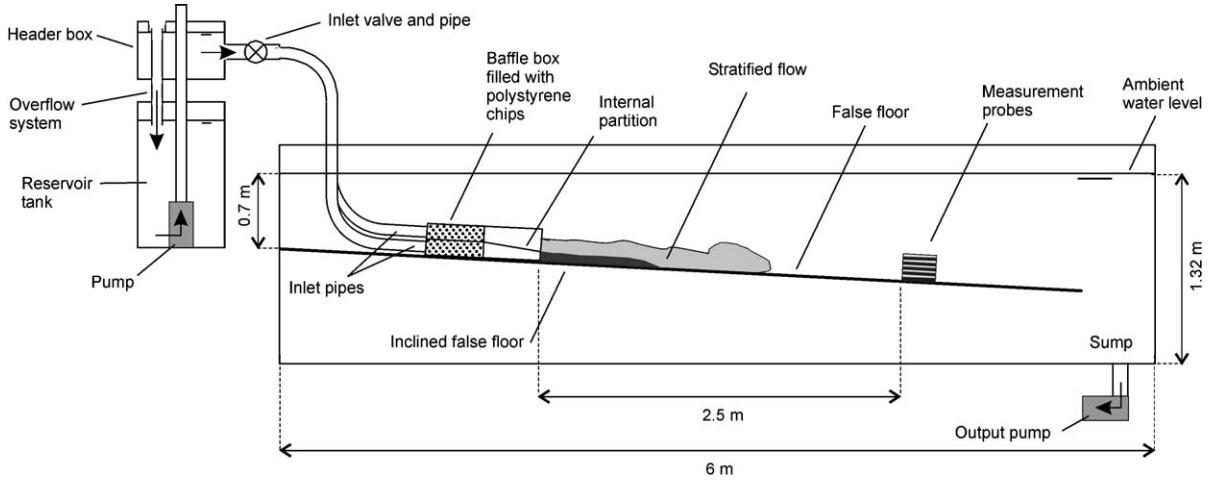

Fig. 3. The experimental set-up used. The apparatus consists of a gravity current tank and two external reservoir tanks. Only one reservoir tank is shown for clarity and is not drawn to scale.

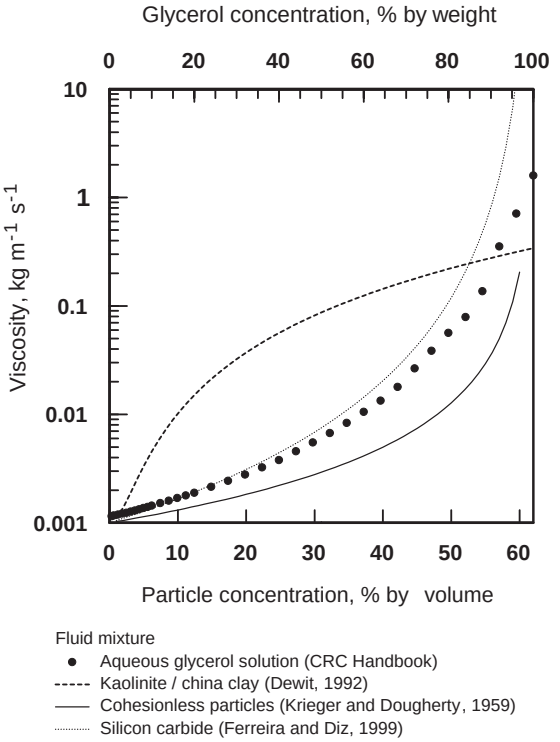

Fig. 4. The relationship between concentration and viscosity for glycerol solutions and several types of particle–water mixtures. The data shown for aqueous glycerol mixtures and china clay bearing mixtures are based on empirical data from the CRC Handbook of Chemistry and Physics and from De Wit (1992), respectively. The relationship for cohesionless mixtures is taken from the theoretical model proposed by Kreiger and Dougherty (1959) for hard spheres suspended in water. The relationship for silicon carbide mixtures is a modified Kreiger and Dougherty model fitted to experimental data of slurries containing particles with a mean particle size of 13 μm and measured at shear rates of ~100 s^{-1} (Ferreira and Diz, 1999).

Coussot, 1997). Density increases linearly with concentration for both aqueous glycerol solutions and particle–water mixtures.

Although aqueous glycerol solutions are excellent analogues for sediment–water mixtures they do not reproduce all aspects that are important to flow behaviour. Aqueous glycerol solutions do not reproduce the influence of non-Newtonian rheology on flow behaviour. In particular, sediment-water mixtures with relatively high concentrations of non-cohesive particles or significant mud content may possess a yield strength and display shear-thickening or shear-thinning behaviour (Barnes, 1989; Coussot, 1997; Major and Pierson, 1992). Of course, the settling of sediment particles and erosion of the substrate is not accounted in experiments using solutions.

3.2. Flow measurements

The flow velocity and concentration were measured at different heights within the flow at a position 2.5 m downstream of the inlet, and the current was filmed at this location. Flow velocity and concentration measuring apparatus were held within a machined holder that ensured individual probes were set parallel both to the bed and to the tank walls.

3.2.1. Flow velocity

The downstream component of flow velocity was measured using ultrasonic Doppler velocity profiling (UDVP). This method derives velocity using the Doppler shift in ultrasound frequency recorded from small particles passing through the measurement volume (Takeda, 1991; Best et al., 2001). The velocity of a particle is given by:

$$U = cf_D/2f_0, \quad (1)$$

where c is the speed of sound in the fluid being investigated, f_D is the Doppler shift and f_0 is the ultrasound frequency. Ultrasonic probes simultaneously measure the velocity in 128 measurement volumes positioned along the length of the ultrasound beam. Flow velocity was recorded upstream of the probes, thus instrumentation placed in the flow did not affect measurements. A vertical array of eight probes was used to measure the downstream velocity at heights of 0.1, 1.9, 2.8, 3.7, 5.7, 7.1, 8.5 and 11.4 cm above the bed. The maximum temporal resolution of the velocity data was 5.8 Hz; other parameters are listed in Table 1.

Velocity data was post-processed to account for the effect of flow concentration on velocity measurements; measurements were affected by variations in glycerol concentration since the speed of ultrasound is a function of concentration. In order to correct data the sound velocity of glycerol solutions was empirically derived using an ultrasonic thickness gauge. The depth was initially measured in water and then again in a solution. The velocity of sound in the solution, c_{sol}, was calculated from

$$c_{sol} = \left(\frac{x_{sol}}{x_{wat}}\right) c_{wat}, \quad (2)$$

Table 1
Starting parameters of the ultrasonic Doppler velocity profilers

Number of probes	8
Height above floor, cm	0.1, 1.9, 2.8, 3.7, 5.7, 7.1, 8.5, 11.4
Ultrasound frequency, MHz	2
Transducer and probe diameter, mm	Two probe sizes used: 5, 8 and 10, 13
Measurement window, mm	12.4–107.1
Measurement bin length, mm	0.74
Velocity resolution, mm s^{-1}	2.3–3.4
Height of nearest measurement bin, mm	6.1 and 11.1
Height of furthest measurement bin, mm	14.35 and 19.4
Ultrasound velocity, m s^{-1}	1480
Sampling frequency/probe, Hz	5.8

The term "bin" refers to a volume in which velocity measurements are recorded.

where c_{wat} is the sound of velocity in water and x_{wat} and x_{sol} is the depth measured in water and the solution, respectively. The velocity of sound of solutions was found to be proportion to glycerol concentration, C, so that $c_{sol}=0.0034C+0.99$. The results show that changes in flow concentration had a relatively small influence (<5%) on flow velocity measurements.

3.2.2. Flow concentration

Flow concentration was measured using an array of five vertically-stacked siphons (internal diameter of 0.6 cm) to extract fluid samples at 0.5, 1.7, 3.0, 5.0 and 8.0 cm above the bed. Fluid samples were collected in beakers positioned on a table on a movable track. During experiments the table was moved to collect samples at 5-s intervals. The concentration of glycerol of each sample was determined by measuring their refractive index using a temperature controlled refractometer. The refractive index, RI, of glycerol solutions is proportional to glycerol concentration, C, and at a temperature of 20 °C, $RI=0.0014C+1.3304$.

The temporal record of concentration may become distorted if the siphon flow rate changes during the experiment, for example due to fluctuation in flow velocity, density, and viscosity. This problem occurred in experiments using relatively high concentrations, ≥80% weight glycerol. In these experiments the discharge per unit time from siphons measuring close to the bed varied by up to five times. Considering changes in the discharge rate, a cumulative offset of several tens of seconds or more over the duration of the time of the flow can be crudely estimated. However, since in these flows an abrupt change in concentration could be clearly identified based on colouration from video recordings, a temporal correction was made to calibrate the measured concentration of the affected siphon. Smaller fluctuations of siphon discharge were observed in other experiments and at measuring positions higher above the bed; however, these were not corrected for.

3.2.3. Reproducibility

The reproducibility of flow velocity and concentration measurements was tested by repeating one experiment using the same starting conditions (Fig. 5). The results indicate standard deviations of 10–25 mm s^{-1} for velocity measurements. These values are calculated by taking a temporal mean over the time period of quasi-steady flow, 0–25 s after the arrival of the flow front. Differences in velocity are relatively large in the probes positioned at 5.7 and 7.1 cm above the bed and at times during the waning flow phase later than 25 s. Trends recorded by the lowest three UDVP probes are broadly similar for the first 20 s. Concentration measurements on average have standard deviations of <3% weight glycerol. A somewhat larger deviation is recorded by the lowest siphon during the initial 10 s (Fig. 5A).

3.3. Experimental runs

A set of experiments were run with the initial starting conditions shown in Table 2. The initial basal-layer concentration (C_L) was increased from ~20% to 90% glycerol whilst the initial upper-layer concentration (C_U) was kept at a low value between 6.5% and 12.3%. Values of glycerol concentration can be compared to the volume fraction, Ø, of sediment–water mixtures based on a comparison of values of kinematic viscosity. On this basis solutions of 10% glycerol are equivalent to volume fraction of cohesionless particles of ~0.2Ø and 20% and 90% glycerol is equivalent to volume fractions of ~0.3Ø and ~0.6Ø, respectively.

3.3.1. Starting stratification

The strength of the stratification of two-layer flows may be assessed using dimensionless ratios whose value if small indicate a strong stratification whilst a value of unity indicates a homogeneous mixture. The

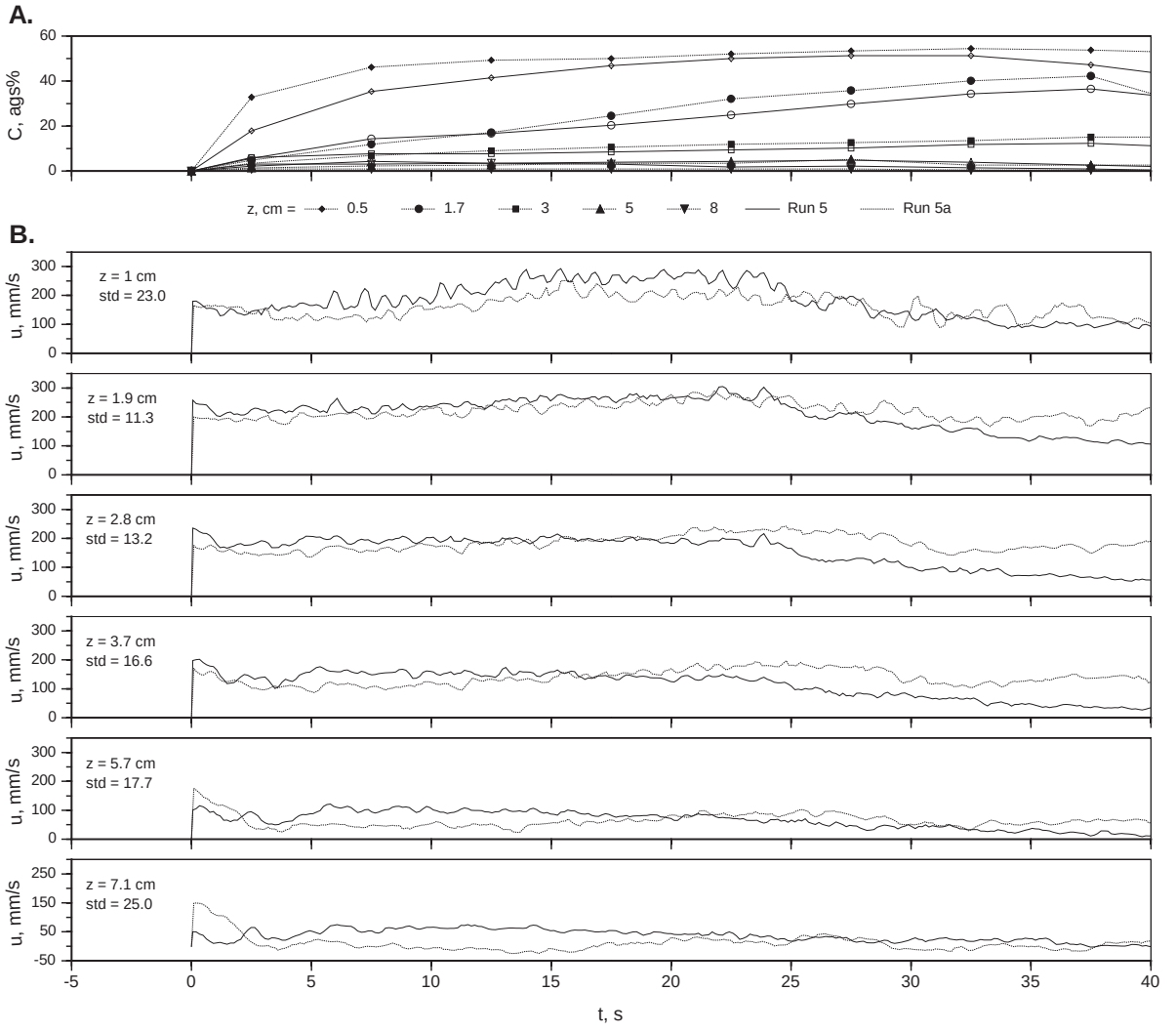

Fig. 5. Concentration (A) and velocity (B) data for multiple runs using the same starting conditions (experiments 5 and 5a). The lower and upper layer had initial glycerol concentrations of ~60% and ~10%, respectively (Table 2). Data show that the reproducibility of data is within ±3% weight glycerol and velocity data is within ±30 mm s^{-1}. Standard deviations were calculated for individual measurement probes using the average standard deviation of measurements taken between 0 and 25 s, during steady input of fluid into the tank. The abbreviations "ags" and "std" are aqueous glycerol solution and standard deviation in mm s^{-1}, respectively.

dimensionless density ratio between layers was defined by Gladstone et al. (2004):

$$\rho^* = \frac{\rho_U - \rho_a}{\rho_L - \rho_a} = \frac{g'_U}{g'_L}, \quad (3)$$

where ρ_L and ρ_U are the densities of the lower and upper layers, respectively, ρ_a is the density of the ambient fluid and the reduced gravity $g' = g(\rho_f - \rho_a/\rho_a)$ where g is the acceleration due to gravity, ρ_f is the density of the flow and ρ_a the density of the ambient fluid. We introduce a dimensionless viscosity ratio defined as

$$\mu^* = \frac{\mu_U - \mu_a}{\mu_L - \mu_a}, \quad (4)$$

where μ_L and μ_U are the viscosities of the lower and upper layers, respectively, and μ_a is the viscosity of the ambient fluid. Gladstone et al. (2004) also defined a

Table 2
Starting parameters of the experiments

Experiment	C_L	C_U	ρ_L	ρ_U	ρ^*	μ_L	μ_U	μ^*	Q_L	Q_U	B^*	T_a	T_L	T_U
1	18.3	9.8	1033.6	1010.9	0.50	0.0020	0.0014	0.446	0.0057	0.005	0.30	11.2	14.4	14.0
2	28.3	10.2	1060.2	1011.9	0.33	0.0026	0.0015	0.331	0.0057	0.005	0.22	10.4	16.6	14.2
3	37.2	6.9	1084.0	1003.1	0.16	0.0038	0.0013	0.116	0.0054	0.005	0.12	11.2	17.6	14.7
4	44.7	8.5	1104.0	1007.4	0.17	0.0054	0.0014	0.096	0.0047	0.005	0.15	10.1	19.3	14.9
5	58.5	9.8	1140.8	1010.9	0.15	0.0120	0.0014	0.038	0.0053	0.005	0.12	10.9	17.6	16.2
5a	59.5	9.4	1143.5	1009.8	0.14	0.0130	0.0014	0.033	0.0054	0.005	0.11	10.4	20.5	14.2
6	67.9	8.5	1165.9	1007.4	0.11	0.0207	0.0014	0.021	0.0054	0.005	0.09	11.6	20.2	15.9
7	79.4	12.3	1196.5	1017.6	0.14	0.0624	0.0015	0.009	0.0030	0.005	0.19	10.5	21.5	15.7
8	87.3	6.5	1217.6	1002.1	0.06	0.1402	0.0013	0.002	0.0020	0.005	0.13	10.7	19.6	15.5
9	88.3	7.7	1220.3	1005.3	0.07	0.1350	0.0014	0.003	0.002	0.005	0.16	11.1	21.1	15.1

The variables are glycerol concentration, C, in percentage by weight; density, ρ, in kg m^{-3}; dimensionless density ratio, ρ^*; viscosity, μ, in kg m^{-1} s^{-1}; dimensionless viscosity ratio, μ^*; discharge, Q, in m^3; and dimensionless buoyancy ratio, B^*. Subscripts a, L and U indicate values for the ambient fluid and lower and upper layers of the current, respectively. Viscosity values are corrected for temperature using the empirical relationship found by Chen and Pearlstein (1987).

ratio for the difference in the driving buoyancy of each layer, B^*, proportional to the layer density and volume. For continuous input flows B^* can be defined as

$$B^* = \frac{Q_U g'_U}{(Q_U g'_U + Q_L g'_L)}, \quad (5)$$

where Q is the discharge per unit width. Values of $0<B^*<0.5$ indicate a greater driving buoyancy in the lower layer, whilst those of $1>B^*>0.5$ indicate a greater driving buoyancy in the upper layer. The starting conditions were chosen to explore a distinct area of the "parameter space" of stratified flows where ρ^*, μ^* and B^* are <0.5 (Table 2). The results from these experiments thus document currents with density ratios of $0.06<\rho^*<0.50$ and viscosity ratios of $0.002<\mu^*<0.48$ and those with a greater driving buoyancy in their lower layer, $0<B^*<0.3$. In order to keep input conditions similar, the upper layer was released slightly, up to 5 s, before the lower layer in experiments 1–8. In two experiments, 9 and 10, the lower layer was released first in order to see how this affected flow behaviour (Table 2).

4. Experimental results

4.1. Visual observations

Gravity currents with a characteristic head and body structure were formed after releasing the glycerol solutions. The two constituent layers were observed to have variable downstream velocities. Thus, two distinct types of current developed with either a faster lower layer or a faster upper layer. In each case the faster layer ran ahead to form the flow front. In some experiments, overtaking of one layer by the other was observed. This occurred within 1 m of the input point and upstream of where flow measurements were recorded. The basal layer, when faster, overtook by pushing lighter fluid of the slower layer upwards and out of the way (Fig. 6A). The upper layer, when faster, overtook by propagating over the relatively slow-moving lower layer (Fig. 6D). The upper layer became progressively thinner and increasingly stretched-out as it moved. On approaching the flow front it intruded into the back of the head along a density interface between the denser fluid of the lower layer and the lighter fluid of the wake. In other experiments overtaking was not observed since the faster layer was released first (Fig. 6B and C). After the flow front had reached the end of the tank floor, a longitudinally uniform current developed, whose two layer stratification was preserved along the length of the tank.

4.1.1. Flows with a fast lower layer

A current with a relatively fast basal layer was formed in experiments run with lower-layer concentrations less than 75% glycerol (experiments 1–6). In these flows fluid from the lower layer formed the head of the current (Fig. 7A). Video recordings show

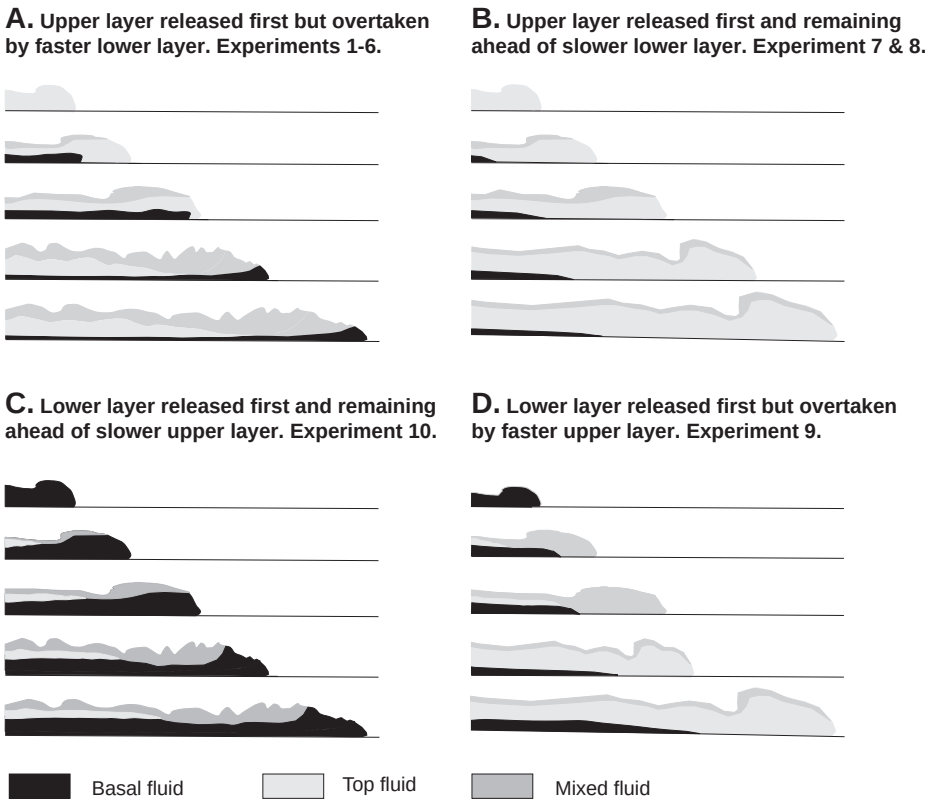

Fig. 6. Schematic diagram showing the evolution of two-layer, stratified gravity currents based on experimental observations. Four types of evolution were observed depending on which layer had a faster velocity and which was released first.

that only a small amount of fluid from the upper layer was able to intrude into the head, instead most of this fluid was swept back into the wake before reaching the flow front. Behind the head, the lower layer had an average thickness of 2–3 cm. The upper layer was thicker, on average being between 6 and 8 cm thick. The interface varied in character between experiments becoming progressively distinct and sharply defined with increasing lower-layer concentration. In all experiments interfacial waves developed and thus the height of the interface varied temporally. In experiments 6 and 7 wave heights were of a similar scale to the thickness of the lower layer. Tracer particles within all flows moved in a turbulent fashion, changing both height above the bed and speed. Mixing was clearly visible between layers. In relatively high-concentration flows (e.g., experiments 5 and 6) mixing occurred in periodic bursts whereby fluid from the denser lower layer was injected upwards into the layer above.

4.1.2. Flows with a fast upper layer

The lower layer was relatively slow compared to the upper layer in experiments run with lower-layer concentrations greater than 75% glycerol (experiments 7 and 8). In these flows the lower layer formed a slow-moving region that lagged behind the current's head. The current's head was formed by fluid fed from the upper layer (Fig. 7B). In experiments 7 and 8 it took the lower layer 8 and 11 s to arrive at the measurement station after the passage of the head, respectively. This slow-moving region had a wedge-shaped front inclined downstream (Fig. 7B). With time, the lower layer achieved a constant thickness of several centimetres. In experiment 7 the interface was noticeably wavy whilst in experiment 8, with the highest glycerol concentration (C_L=90%), the interface between the two layers was flat. Many of the tracer particles were observed to become concentrated at the interfacial boundary. For experiment 8, those

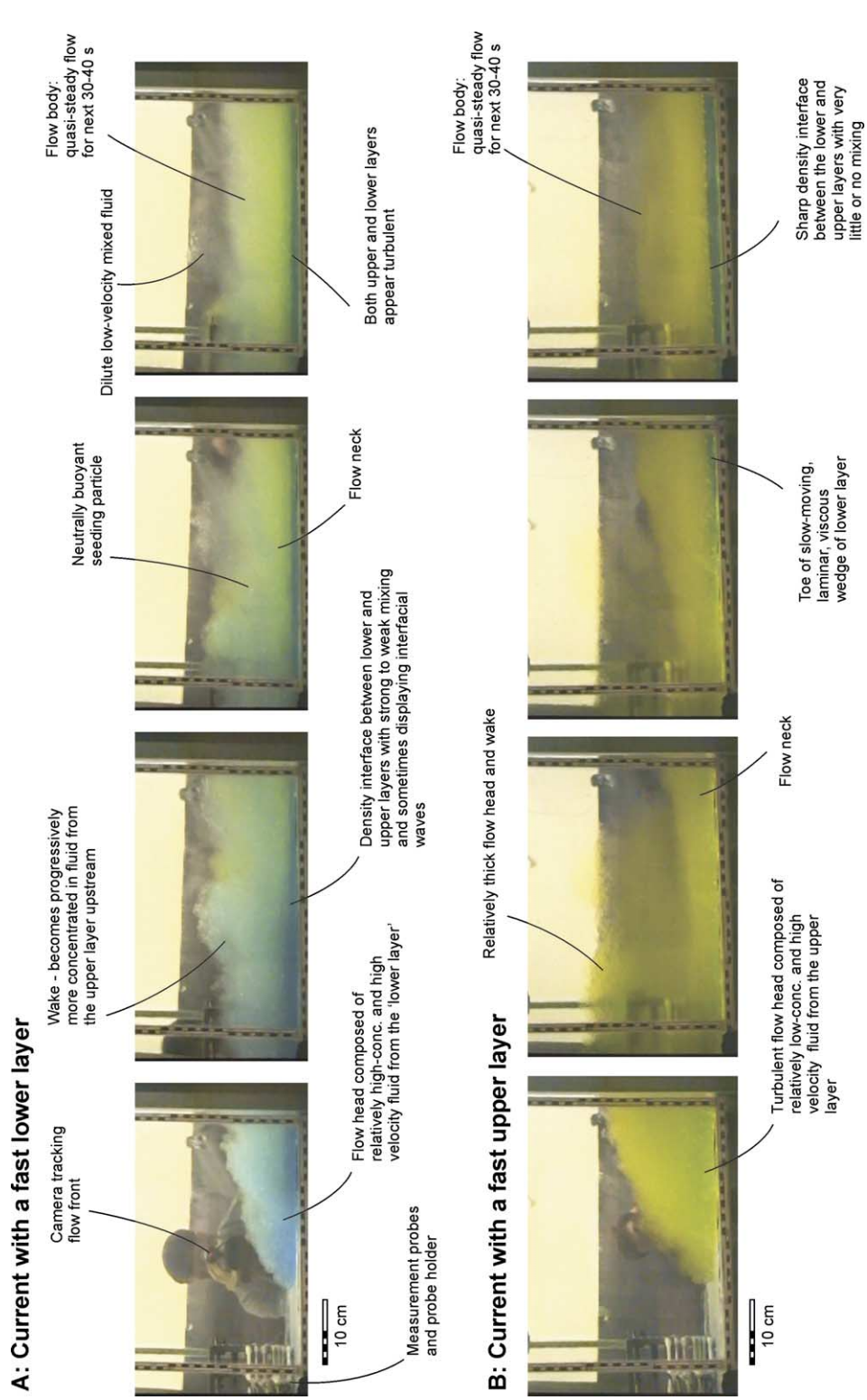

Fig. 7. Successive photos taken at a position of 2.5 m downstream of the inlet point. (A) A current with a relatively fast lower layer (experiment 3). Photographs were taken at 2-s intervals. (B) A current with a relatively fast upper layer and a relatively slow, laminar-moving lower layer that lags behind the flow front (experiment 8). Photographs were taken every 4 s.

tracer particles on the boundary and within the lower layer were observed to move in a laminar fashion whereby they maintained a constant speed and moved in a straight line at a constant height above the bed. Mixing between the two layers, especially in experiment 8, appeared to be suppressed. However, fluid of a colour indicative of mixing and moving relatively fast was observed preceding the arrival of the lower layer.

4.2. Velocity and concentration profiles

Maps of flow velocity and concentration through time and for different heights above the bed are shown in Fig. 8. These plots show that currents achieved quasi-steady conditions for both flow velocity and concentration for a period of 10 s or more. The initial recorded flow velocity and concentration, however, are unsteady and typically waxing for the first 5 to

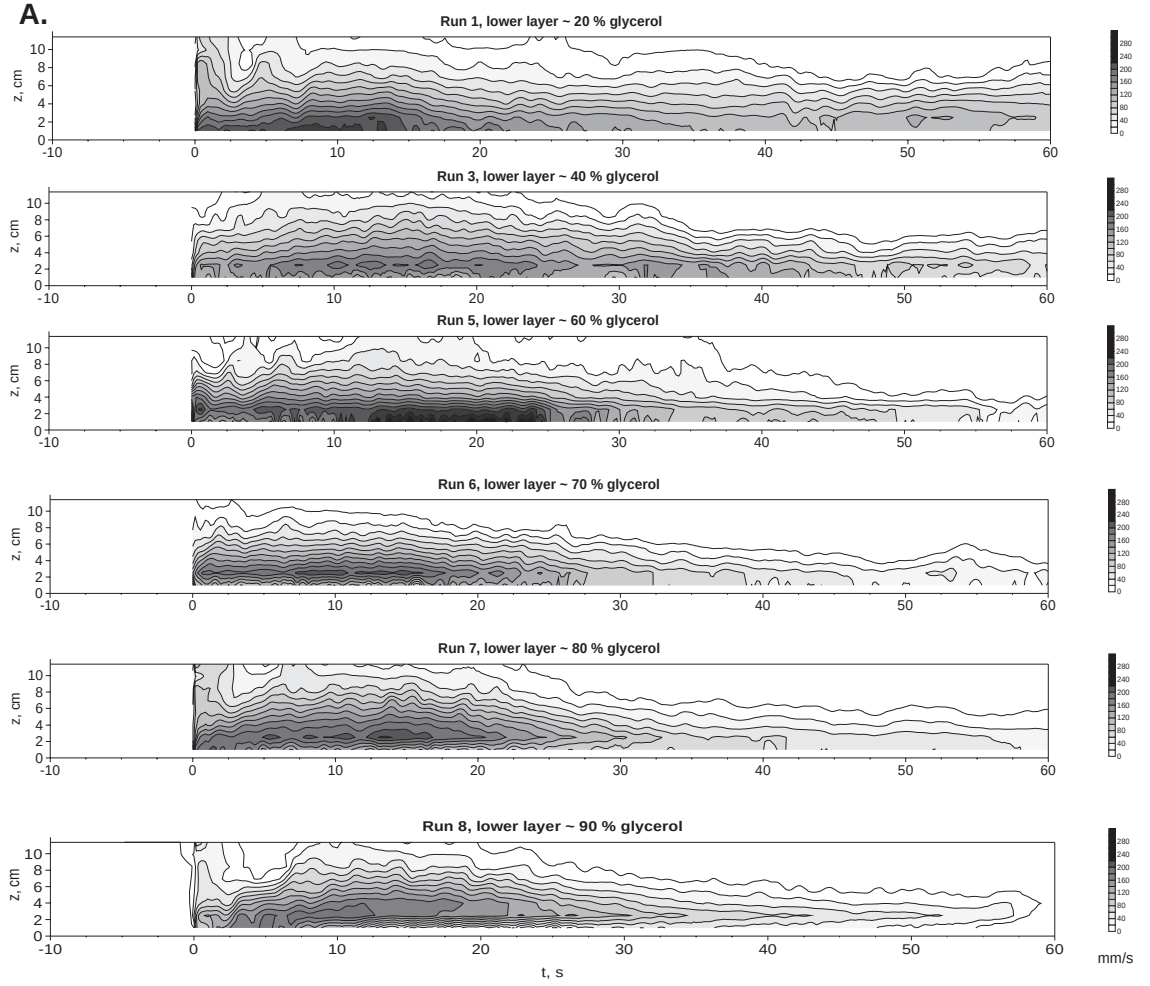

Fig. 8. (A) Maps of flow velocity constructed from temporal measurements taken at eight heights (z) above the bed and at a position of 2.5 m downstream of the inlet point for selected experiments. Data shown is the mean velocity of 60 bins and three successive cycles. (B) Maps of flow concentration constructed from temporal measurements taken at five heights (z) above the bed and at a position of 2.5 m downstream of the inlet point for selected experiments. The time, t, is measured in seconds after the arrival of the flow front. Measurements show quasi-steady flow conditions for limited periods of time some 5 to 20 s after the arrival of the flow front. Experiments 1, 3, 5 and 6 had a relatively fast, high-concentration lower layer. Experiments 7 and 8 had a relatively slow-moving, high-concentration, lower layer.

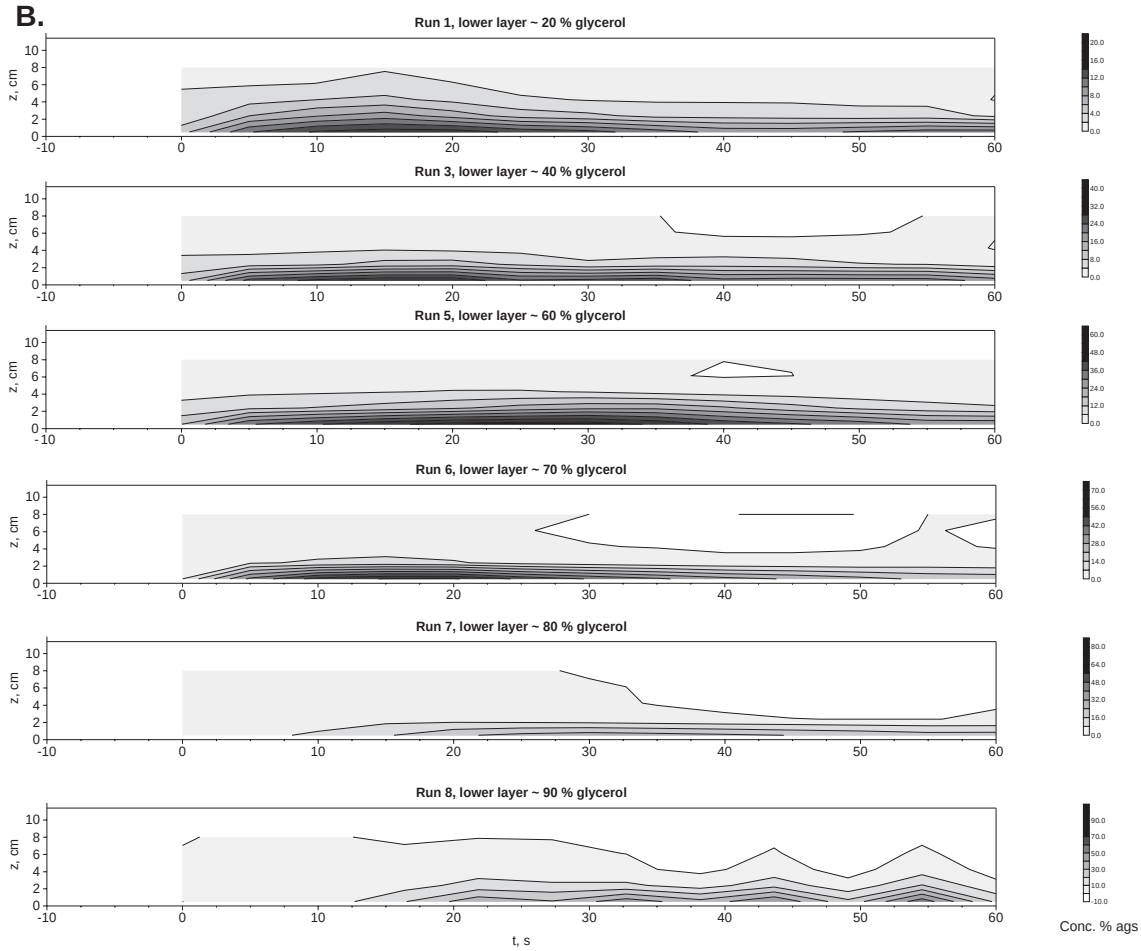

Fig. 8 (*continued*).

15 s (Fig. 8). This is most apparent in the lower part of the flow immediately above the bed. Flow unsteadiness at these times is related to the passage of the current's head and subsequent large-scale eddies. Currents began to wane after about 20 s marking the time at which the input supply was turned off (Fig. 8). The waning of flows becomes noticeably stronger with increasing lower-layer concentration.

4.2.1. Flows with a fast lower layer

Experimental flows 1–6 with fast moving bases are characterised by temporal concentration and velocity profiles that mirror one another in that maximum and minimum values occur at similar times (Fig. 8). Near-bed velocities and concentrations tend to increase with time to a quasi-steady state before waning (Fig. 9). Maximum measured velocities of ~300 mm s^{-1} occurred in experiments 6 and 7 with lower-layer glycerol concentrations of 60% and 70%, respectively. Vertical profiles in the body (Fig. 10) are similar to those described for other low-concentration currents (Fig. 2A–B); concentration displays continuous or nearly continuous profiles whilst velocity has a concave upward-facing shape above the velocity maximum (Fig. 10A–D). The velocity maximum occurs between 1 to 2 cm above the bed and at a fraction of 0.1–0.15 of the total flow depth. The velocity maximum in experiments 1 to 6 occurs at a similar height to the interfacial boundary between layers. Root-mean-squared (RMS) values of the temporal velocity

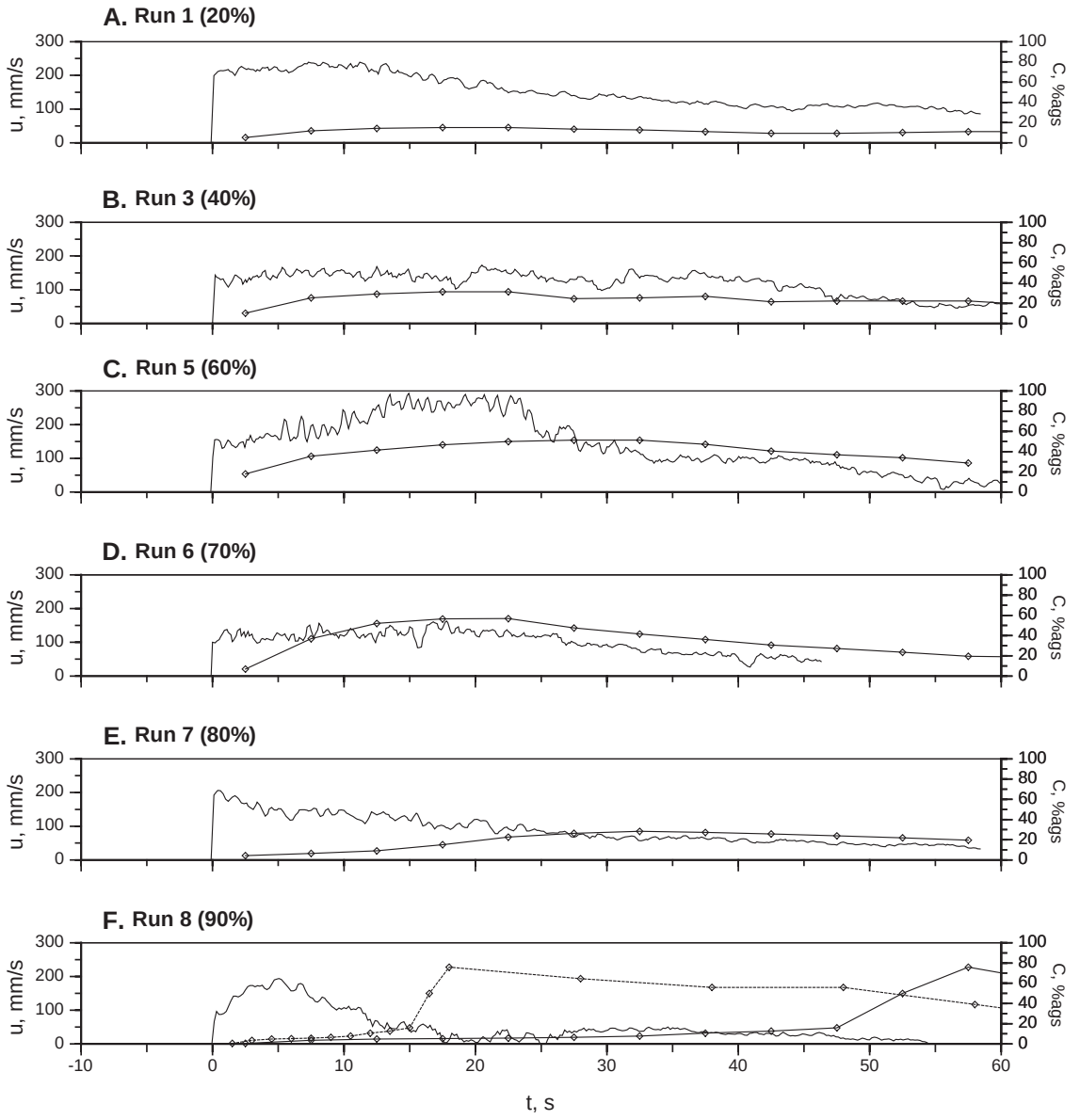

Fig. 9. (A–F) Temporal profiles of velocity and concentration measured at 1 cm and 0.5 cm above the bed, respectively, and at a position of 2.5 m downstream of the inlet point, for selected experiments. The time, t, is measured in seconds after the arrival of the flow front. The dashed line of flow concentration for experiment 8 shows data that have been corrected for temporal displacement resulting from variable siphon flow rates. See text for further explanation.

time-series, a proxy for flow turbulence, have maximum values close to the bed and show a decrease upwards away from the bed. This type of distribution has been observed in other quasi-steady turbulent density currents (e.g., Buckee et al., 2001).

4.2.2. Flows with a fast upper layer

The temporal and vertical profiles of experimental currents 7 and 8 with slower moving lower layers are markedly different to those with faster ones. In these currents the flow velocity and con-

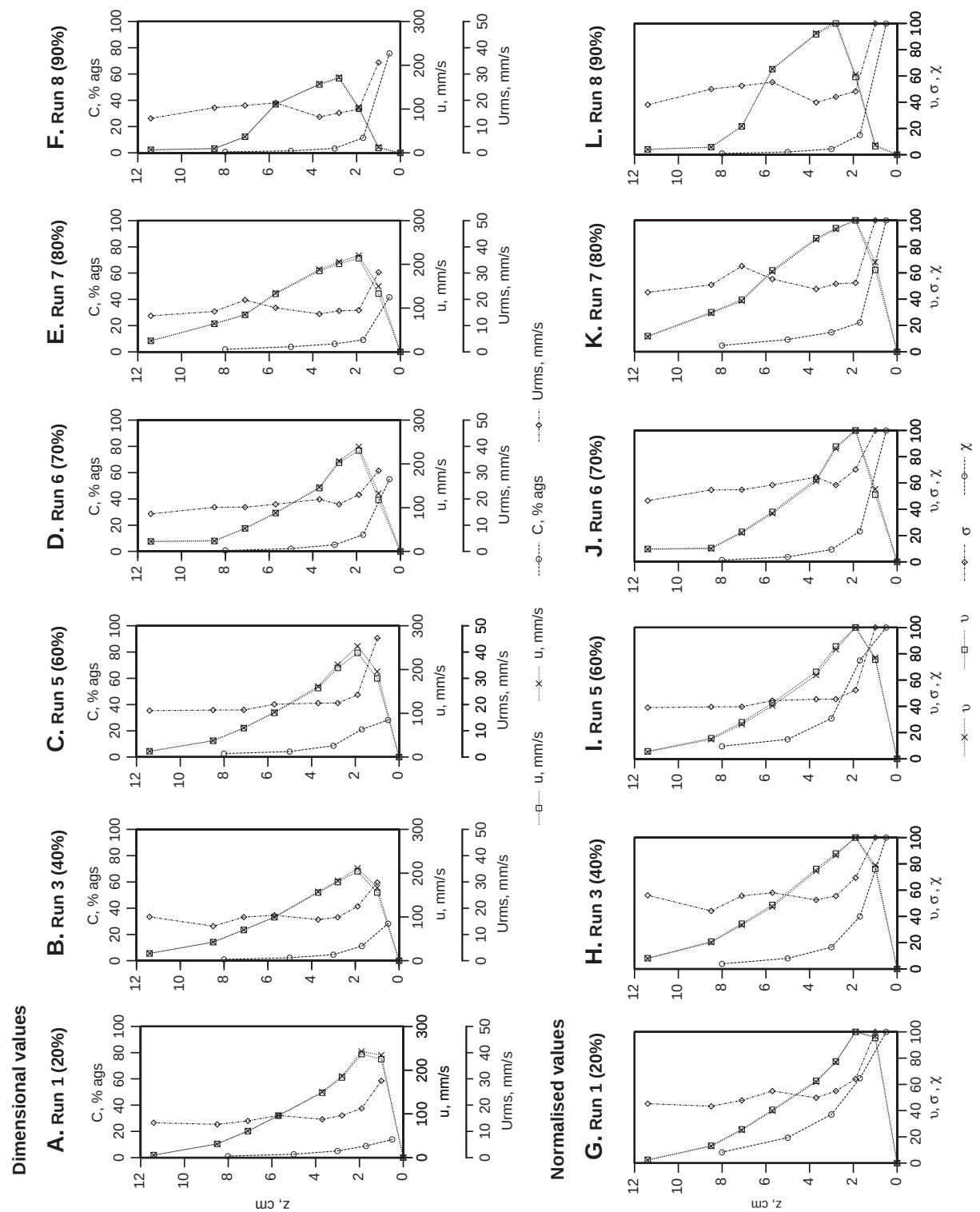
Dimensional values
A. Run 1 (20%)
B. Run 3 (40%)
C. Run 5 (60%)
D. Run 6 (70%)
E. Run 7 (80%)
F. Run 8 (90%)
Normalised values
G. Run 1 (20%)
H. Run 3 (40%)
I. Run 5 (60%)
J. Run 6 (70%)
K. Run 7 (80%)
L. Run 8 (90%)
z, cm
C, % ags
u, mm/s
Urms, mm/s
υ, σ, χ
u, mm/s
C, % ags
Urms, mm/s
υ
σ
χ

centration do not mimic one another (Fig. 8). Near bed velocities increase with time and then decrease whilst concentration is initially low before increasing (Fig. 9). In experiment 8 an abrupt increase in flow concentration is seen at about 15 s, marking the arrival of the slow-moving lower layer (Fig. 9F). An area of enhanced flow velocity also occurs several centimetres above the bed before the arrival of the slow-moving lower layer at 7–12 s (Fig. 8). Initial flow unsteadiness is related to the passage of the head but also to their longitudinal structure. Vertical concentration profiles of experiments 7 and 8 display a less gradual and more step-like stratification than experiments with lower concentrations, e.g. experiments 1 and 3 (Fig. 10E–F). Currents with a slow moving lower layer have a convex shaped velocity distribution above the maximum being quite different to those recorded for experiments 1–6. Also in experiment 8, the velocity maximum is relatively high in the flow and it is situated in the upper-layer at a fractional depth of between 0.3 and 0.4 (Fig. 10L). This velocity distribution is similar to those of high-concentration suspension flows reported by Postma et al. (1988). RMS values of the temporal velocity time-series show profiles and values similar to currents with a faster lower layer; maximum values occur close to the lower flow boundary and values decrease upwards. The high RMS values recorded near the bed are surprising, especially for experiment 8, since visual observations suggest that the lower layer moved in a laminar fashion. Since the velocity measurements taken by the lowest position probe were taken from an area close to the interfacial boundary between layers, we suggest that the high RMS values are caused by turbulence related to the interfacial boundary. Alternatively, conditions close to the tank wall may have been different to those in the centre of the tank where the data were recorded; the interfacial boundary may have been lower or the lower layer more turbulent in the centre of the tank.

5. Discussion

The experiments show that the behaviour of continuously-fed gravity currents is strongly controlled by their stratification. Initial flow unsteadiness is related to the passage of the head, but also to the current's longitudinal structure. In the ranges of ρ^*, μ^* and B^* (all <0.5) investigated, two distinct types of behaviour were observed. A summary of the characteristics of each current type is shown in Fig. 11. Those with low to moderate maximum concentrations, <75% glycerol, have fast-moving, high-concentration, basal regions (Fig. 11A). In contrast, currents with relatively high maximum concentrations, >75% glycerol, have a slow moving basal region that lags behind the flow front (Fig. 11B). Particle-laden laboratory currents with similar flow structures to these two types have been observed previously. Flows with high-concentration fast-moving bases have been noted by Hampton (1972), Mohrig et al. (1998) and Marr et al. (2001), whilst currents with slow moving bases have been observed by Postma et al. (1988).

5.1. Interpretation of flow behaviour

We interpret the observed change in behaviour to correspond to a transition in the flow dynamics of the lower layer from being inertia-driven to viscosity-controlled. A reduction in the lower layer velocity at concentrations exceeding 75% glycerol can be explained by the enhanced drag at the lower flow boundary, a characteristic of high viscosity flows. The dimensionless Reynolds number (Re) is a measure of the ratio of inertial to viscous forces and may be used to assess the transition between turbulent and laminar flow regimes. The Reynolds number is evaluated here using

$$Re = \frac{uh\rho}{\mu} \tag{6}$$

where u is a velocity scale, h is a length scale and ρ and μ are the density and viscosity of the fluid, respectively. The drag force experienced by flows

Fig. 10. (A–F) Vertical profiles of the downstream velocity (u), the root-mean-square of downstream velocity (U_{rms}) and the concentration (C) for selected experiments. Profiles are taken from the body of currents at 10 s after the arrival of the flow front except the profile for Run 8 which was taken at 20 s. Velocities indicated by crosses show values corrected for fluid density (see text) whilst those indicated by squares show uncorrected values. (G–L) Non-dimensional values given as a percentage of the maximum value in each profile; downstream velocity (υ), root-mean-square of downstream velocity (σ) and concentration (χ).

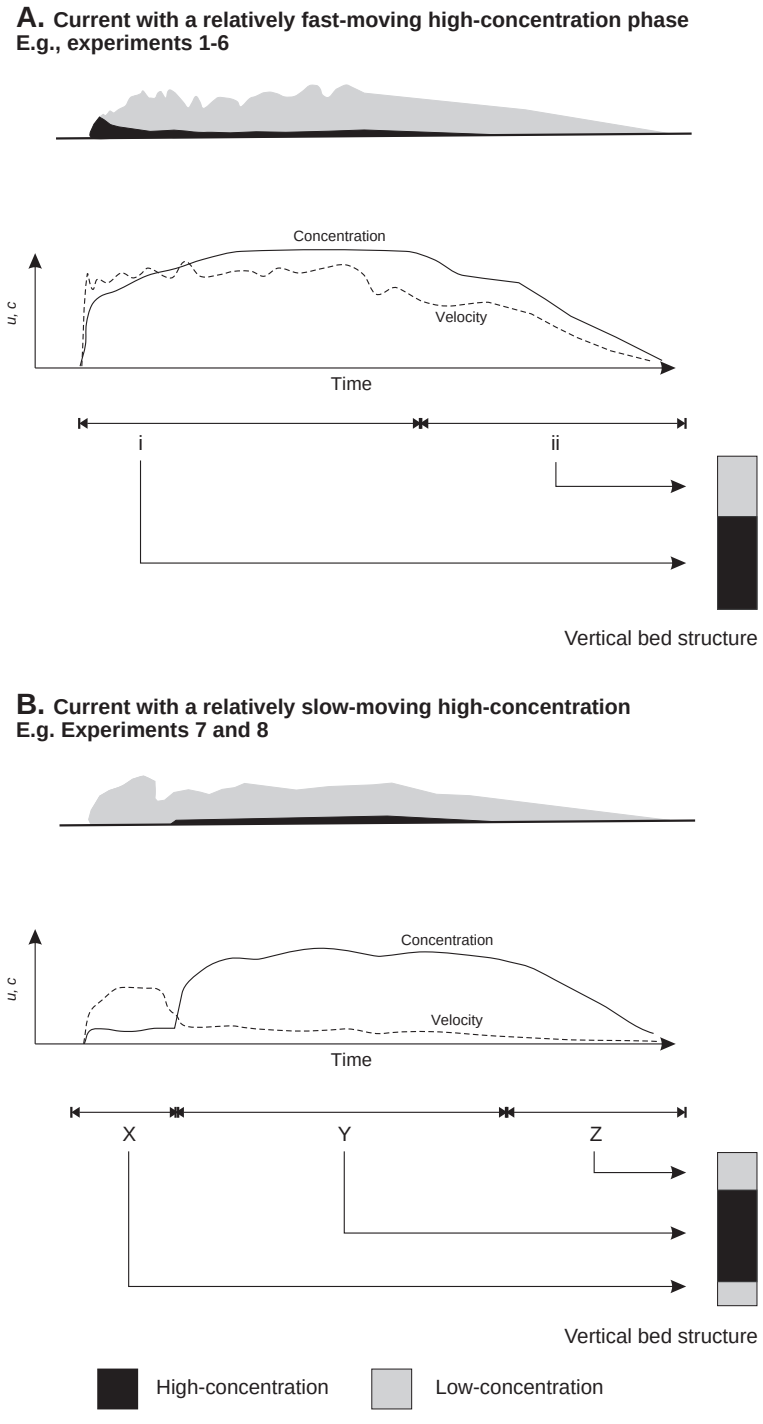

Fig. 11. Summary diagram of experimental data showing the two different current types observed. (A) A current with a relatively fast-moving, high-concentration lower layer that also forms the flow front. (B) A current with a relatively fast-moving, high-concentration upper layer. The lower-layer lags behind the flow front. For each current type the near-bed temporal trends of velocity and concentration and corresponding inferred depositional sequence at a single location is shown.

varies with Reynolds number. The amount of drag is similar in turbulent flows with relatively high Reynolds numbers but increases significantly at smaller Reynolds numbers in the range of transitional and laminar flow conditions. This relationship between drag and Reynolds number is known to apply to pipe flow (Chadwick and Morfett, 1992). van Kessel and Kranenburg (1996) showed that the drag coefficient varies strongly at low Reynolds numbers, $Re < 10^3$, for gravity currents of fluid-mud (Fig. 12).

The Reynolds number of gravity currents is usually deduced using the bulk current properties to yield a single value for the whole current. Since viscosity-stratified currents may exhibit both laminar and turbulent flow at different heights above the bed, the application of a single Reynolds number may not be appropriate. One way to assess the flow character of strongly stratified currents is to calculate separate Reynolds numbers for regions near the bed and higher up in the flow (Table 3A). Reynolds numbers were calculated for below ($Re_{<U_{max}}$) and above ($Re_{>U_{max}}$) the velocity maximum using measured flow properties

$$Re = \frac{UhP}{M}, \tag{7}$$

where U, P, and M are the layer depth-average velocity, concentration, and viscosity respectively, and h is the layer depth (Table 3A). Various values of the Reynolds number have been proposed for the threshold between laminar to turbulent flow ranging over one order of magnitude. However, laboratory studies often take the transitional number as 500–2000 (Simpson and Britter, 1979; Allen, 1985). This threshold is also used in this study and given the range of values calculated for the experimental currents, would appear to be a reasonable approximation. Values above the velocity maximum fall into the turbulent regime, $3000 < Re < 12\,000$, corresponding to observations of turbulent particle movement in the upper part of the flow. Smaller values of the Reynolds number characterise the region below the velocity maximum. Importantly, they show a decrease from 2500 to 900 Re with increasing glycerol concentration. These Reynolds numbers fall into the range where values of drag are expected to vary strongly and support our interpretation of a varying drag influence at the lower flow boundary. The flow Reynolds numbers calculated are subject to some measurement error in flow concentration. The value of the Reynolds number below the velocity maximum for experiment 7 (with the second highest glycerol concentration) is spuriously high at 1600 compared to values for flows of similar concentration. This corresponds to relatively low values of glycerol concentration recorded for this flow and is likely to be an artefact of selective siphoning of fluid with a lower concentration and viscosity. Reynolds numbers calculated using the initial values of fluid density and viscosity for the lower layer (Re_L), may therefore give a better estimate for high-concentration flows in which mixing was unimportant (Table 3B). These values indicate Reynolds numbers for the high-concentration flows of <100, consistent with visual observations of laminar particle movement in these currents.

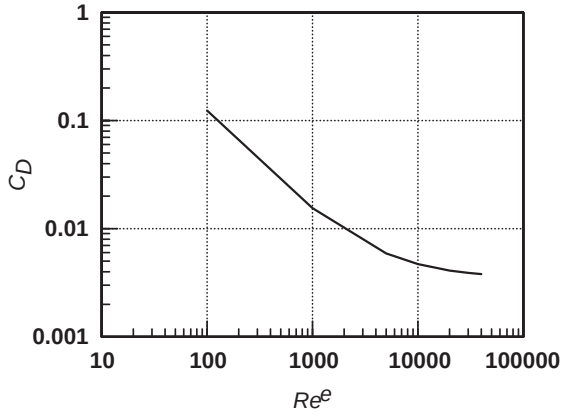

Fig. 12. Drag coefficient, C_D, as a function of the effective Reynolds number, Re^e, for fluid mud gravity currents presented by van Kessel and Kranenburg (1996). Their original data is approximated by the curve $C_D \sim (12+0.1Re^e)/Re^e$, where Re^e is an effective Reynolds number (see Eq. (11) in van Kessel and Kranenburg, 1996). The graph shows that drag increases significantly at low Reynolds numbers and in the range below turbulent flow conditions, $Re^e < 3000$, using the criterion proposed by Liu and Mei (1990).

5.2. Stratified flow regimes

Based on experimental data, Gladstone et al. (2004) constructed a flow regime diagram for the behaviour of two layer, stratified currents of various density ratios, ρ^* and buoyancy ratios, B^* (Fig. 13A). In their scheme, the layer buoyancy determines which layer runs ahead to form the leading edge of the flow; the lower and upper layers run ahead when $B^* < 0.5$ and $B^* > 0.5$, respectively. All the currents studied

Table 3
Calculated flow characteristics for laboratory experiments

A. Parameters based on depth-averaged values and U_{max} subdivision

Experiment	U_C	h_C	P_C	M_C	Re_C	Fr	Ri_B	$U_{<U_{max}}$	$h_{<U_{max}}$	$P_{<U_{max}}$	$M_{<U_{max}}$	$Re_{<U_{max}}$	$U_{>U_{max}}$	$h_{>U_{max}}$	$P_{>U_{max}}$	$M_{>U_{max}}$	$Re_{>U_{max}}$
1	0.10	0.13	994.1	0.0011	11,768	1.1	0.9	0.154	0.02	1004.9	0.0012	2513	0.08	0.11	992.2	0.0011	7768
2	0.10	0.13	1000.6	0.0012	10,510	0.7	1.3	0.136	0.02	1017.5	0.0014	2034	0.09	0.11	997.5	0.0011	8486
3	0.11	0.13	997.4	0.0011	12,069	1.0	1.0	0.116	0.02	1025.5	0.0015	1553	0.09	0.11	992.3	0.0011	9000
4	0.10	0.13	995.1	0.0011	11,598	1.0	1.0	0.130	0.02	1027.3	0.0016	1635	0.08	0.11	989.3	0.0011	8360
5	0.11	0.13	1003.5	0.0012	11,732	0.8	1.3	0.135	0.02	1025.5	0.0015	1800	0.09	0.11	999.5	0.0012	8388
6	0.10	0.13	1003.6	0.0012	10,990	0.7	1.4	0.105	0.02	1064.2	0.0026	847	0.09	0.11	992.6	0.0011	8873
7	0.13	0.13	1001.9	0.0012	14,539	1.0	1.0	0.135	0.02	1044.9	0.0017	1623	0.11	0.11	994.1	0.0011	11,266
8	0.07	0.10	1011.0	0.0013	5522	0.5	2.1	0.095	0.03	1094.1	0.0037	855	0.06	0.07	991.1	0.0011	3664

B. Parameters based on initial starting values and layer subdivision

Experiment	U_C	h_C	ρ_C	μ_C	Re_C	Fr	Ri_B	$U_{<U_{max}}$	h_L	ρ_L	μ_L	Re_L	$U_{>U_{max}}$	h_U	ρ_U	μ_U	Re_U
1	0.10	0.13	1014.4	0.0015	8804	0.5	1.8	0.154	0.02	1033.6	0.0020	1622	0.08	0.11	1010.9	0.0014	6012
2	0.10	0.13	1019.4	0.0017	7470	0.5	2.1	0.136	0.02	1060.2	0.0026	1114	0.09	0.11	1011.9	0.0015	6454
3	0.11	0.13	1015.6	0.0017	8305	0.6	1.8	0.116	0.02	1084.0	0.0038	669	0.09	0.11	1003.1	0.0013	7497
4	0.10	0.13	1022.3	0.0020	6559	0.5	2.1	0.130	0.02	1104.0	0.0054	531	0.08	0.11	1007.4	0.0014	6303
5	0.11	0.13	1030.9	0.0031	4796	0.5	2.2	0.135	0.02	1140.8	0.0120	255	0.09	0.11	1010.9	0.0014	6994
6	0.10	0.13	1031.8	0.0044	3129	0.4	2.3	0.097	0.02	1165.9	0.0207	109	0.09	0.11	1007.4	0.0014	6925
7	0.13	0.13	1045.1	0.0109	1666	0.5	2.0	0.135	0.02	1196.5	0.0624	52	0.11	0.11	1017.6	0.0015	8368
8	0.07	0.10	1066.7	0.0430	176	0.3	3.9	0.095	0.03	1217.6	0.1402	25	0.06	0.07	1002.1	0.0013	3022

(A) Flow characteristics calculated using depth-averaged values for the whole current and for portions of the current above and below the velocity maximum. Variables are: depth-averaged velocity, U, in m s^{-1}; height, h, in m; depth-averaged density, P, in kg m^{-3}; viscosity, M, in kg m^{-1} s^{-1}; dimensionless Reynolds number, $Re = U_C P h/M$; dimensionless Froude number, $Fr = U_C/(h_C(gP - \rho_0/\rho_0)^{1/2}$ (where g is the acceleration due to gravity and ρ_0 is the density of the ambient fluid); and dimensionless Richardson number, $Ri_B = 1/Fr$. Subscripts C, $>U_{max}$ and $<U_{max}$ indicate values for the whole current, and the portion of the current below and above the velocity maximum, respectively. Current height, h_C, was estimated from photos. The height of the velocity maximum was estimated using velocity measurements (Fig. 10). (B) Flow characteristics calculated using initial values for the whole current and for upper and lower layers. Variables are: depth-averaged velocity, U, in m s^{-1}; height, h, in m; layer density, ρ, in kg m^{-3}; viscosity, μ, in kg m^{-1} s^{-1}; dimensionless Reynolds number, $Re = U_C \rho h/\mu$; dimensionless Froude number, $Fr = U_C/(h_C(g\rho_C - \rho_0/\rho_0)^{1/2}$; and dimensionless Richardson number, $Ri_B = 1/Fr$. Subscripts L, U and C indicate values for lower and upper layers and whole current, respectively. Note that the velocity values used are the same in both A and B.

here had a greater buoyancy in their lower layer with values of $B^* < 0.5$. Experiments 1 to 6 with a relatively fast-moving lower layer displayed behaviour consistent with the findings of Gladstone et al. (2004) for inertial, lock-release currents. In experiments 7 and 8, the lower layer was relatively slow-moving compared to the upper layer, despite it having a much greater driving force, $B^* < 0.2$. This indicates that the flow buoyancy does not control flow behaviour in currents with strong viscosity stratification μ^* (of the order of 1×10^{-3} in the present experiments). Hence, a third axis to Gladstone et al.'s proposed regime diagram may be added to describe currents with varied viscosity stratification (Fig. 13B).

The second axis of the regime diagram constructed by Gladstone et al. (2004) indicates relative amounts of mixing between layers based on ρ^*; for currents with $\rho^* < 0.4$ the initial stratification is maintained whilst for those with $\rho^* > 0.4$ stratification is quickly destroyed by mixing. Comparison between the present experiments and those of Gladstone et al. (2004), in terms of ρ^*, however, is not straightforward for several reasons. Firstly, the degree of mixing in continuous-flux flows will be significantly different to surge-type flows since the latter is dominated by the dynamics of the current's head. Secondly, the entire duration of flow in Gladstone et al.'s study was observed from the point of initiation to their arrest whereas in the present experiments, currents could not be observed to their natural stopping point. Bearing this in mind, it was observed that in all flows with density ratios <0.35, the initial two layer stratification was maintained, this being consistent with Gladstone et al. (2004) results.

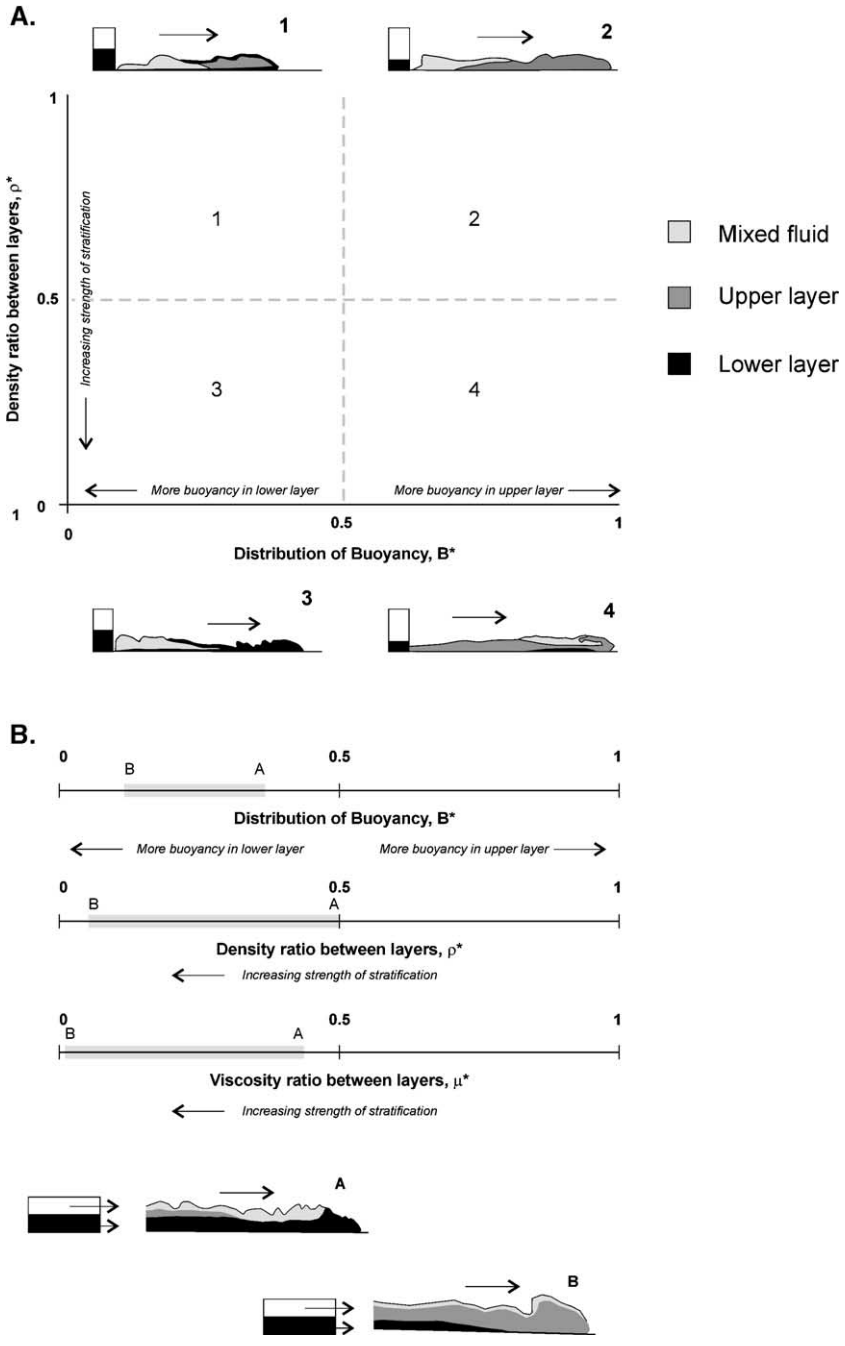

Fig. 13. (A) Regime diagram constructed by Gladstone et al. (2004) summarising the behaviour of two-layer density-stratified, surge-type currents. The graph describes currents in terms of the dimensionless parameters density ratio ρ^* and distribution of buoyancy B^*. Modified from Gladstone et al. (2004). (B) Diagram showing the parameter space varied in the present set of experiments in terms of the three dimensionless parameters, density ratio ρ^*, distribution of buoyancy B^* and viscosity ratio μ^*. The range in these parameters explored is shaded. Schematic cartoons for current behaviour are shown for different regimes of flow behaviour.

5.3. Implications for deposit character

The vertical characteristics of sediment gravity flow deposits are controlled by temporal variations in flow velocity and concentration at a point, and thus, by the stream-wise structure of the current (Branney and Kokelaar, 2002; Kneller and McCaffrey, 2003; McCaffrey et al., 2003; Choux et al., 2005—this issue). The experimental data show that stratified flows with relatively fast and slow-moving lower layers have markedly different near-bed temporal trends in flow properties (Figs. 9 and 10). Assuming natural sediment-laden flows also display these current structures, it follows that several distinct bed types should be deposited. Here we speculate on the characteristics of these beds, and propose two simple depositional models for stratified sediment-laden currents (Fig. 11). These models assume deposition occurs throughout the passage of the head, body and tail of the flow and at a single location. The models developed should be considered as 'ideal' deposit types. As for other models, such as the Bouma sequence, variations should be expected given the range of controlling factors on the final deposit character.

5.3.1. Deposit interpretation

In order to identify the deposits of stratified submarine currents, sedimentary features that reliably record deposition by flows of low and high sediment concentration need to be defined. This has been a controversial subject, especially with regard to the interpretation of massive sandstones (see discussions in Kneller and Buckee, 2000; Mulder and Alexander, 2001; Amy et al., 2005—this issue). Gradual deposition of particles from a relatively low sediment-concentration phase (turbidity current) may be recognised by the presence of tractional bedforms, vertical normal grading under waning flow conditions and a high degree of grain-size sorting within the deposit. However, structureless intervals such as the Bouma T_a division may be produced under relatively high sediment-load fallout rates leading to the suppression of traction (Arnott and Hand, 1989). In circumstances of steady flow the T_a division may also lack grading (Kneller, 1995). Deposition from a high-concentration phase (debris flow) occurring by en masse settling will also tend to produce ungraded beds. However, given a wide grain-size distribution (mud to centimetre clasts), debris flow deposits will be distinctive from Bouma T_a divisions on account of their poor sorting, relatively high matrix mud contents and randomly distributed outsized clasts. In addition debrites may display a distinct shear fabric. These criteria follow those used by others (e.g., Lowe, 1982; Ghibaudo, 1992; Mulder and Alexander, 2001).

5.3.2. Deposits from flows with fast-moving high-concentration phases

Particle-laden currents with relatively fast moving, high-concentration phases will have an initial phase of deposition from flow with relatively high sediment concentrations followed later by deposition from flow with lower sediment concentrations. The resulting depositional sequence will comprise a high-concentration flow deposit overlain by a low-concentration flow deposit (Fig. 11A). Beds displaying this type of vertical character and ranging from several metres to over tens of metres in thickness are commonly exposed in the Eocene/Oligocene sedimentary sequence of the Grès de Peïra Cava Formation, SE France (Fig. 14A). These sediments were deposited in a relatively small (tens of kilometres long and wide) deep-water basin in which flows were confined by the local basin bathymetry (Hilton, 1994; Amy, 2000; McCaffrey and Kneller, 2001; Amy et al., 2004). In relatively proximal sections, many beds contain a coarse-grained (small-pebble to very coarse sand grade), very poorly sorted, clast-rich basal interval. The basal portion of these beds is interpreted as having been deposited from a high sediment-concentration flow phase. The mud content varies laterally in the basal interval, implying that the cohesive strength of the flow may have varied locally. The upper part of the beds is finer grained and better sorted and displays normal grading and usually current lamination. The upper parts of beds are interpreted to record deposition from a relatively low-concentration portion of the current deposited after the high-concentration phase had passed. Correlations indicate that these are the deposits of single flow events and not an amalgamated sequence produced by multiple flows of different particle concentrations (Amy, 2000).

5.3.3. Deposits from flows with slow-moving high-concentration phases

Particle-laden currents with relatively slow-moving, high-concentration phases will deposit initially from flow with low to intermediate sediment concentrations, followed by deposition from flow with high sediment concentrations and finally from the trailing flow with relatively low sediment concentrations. At a

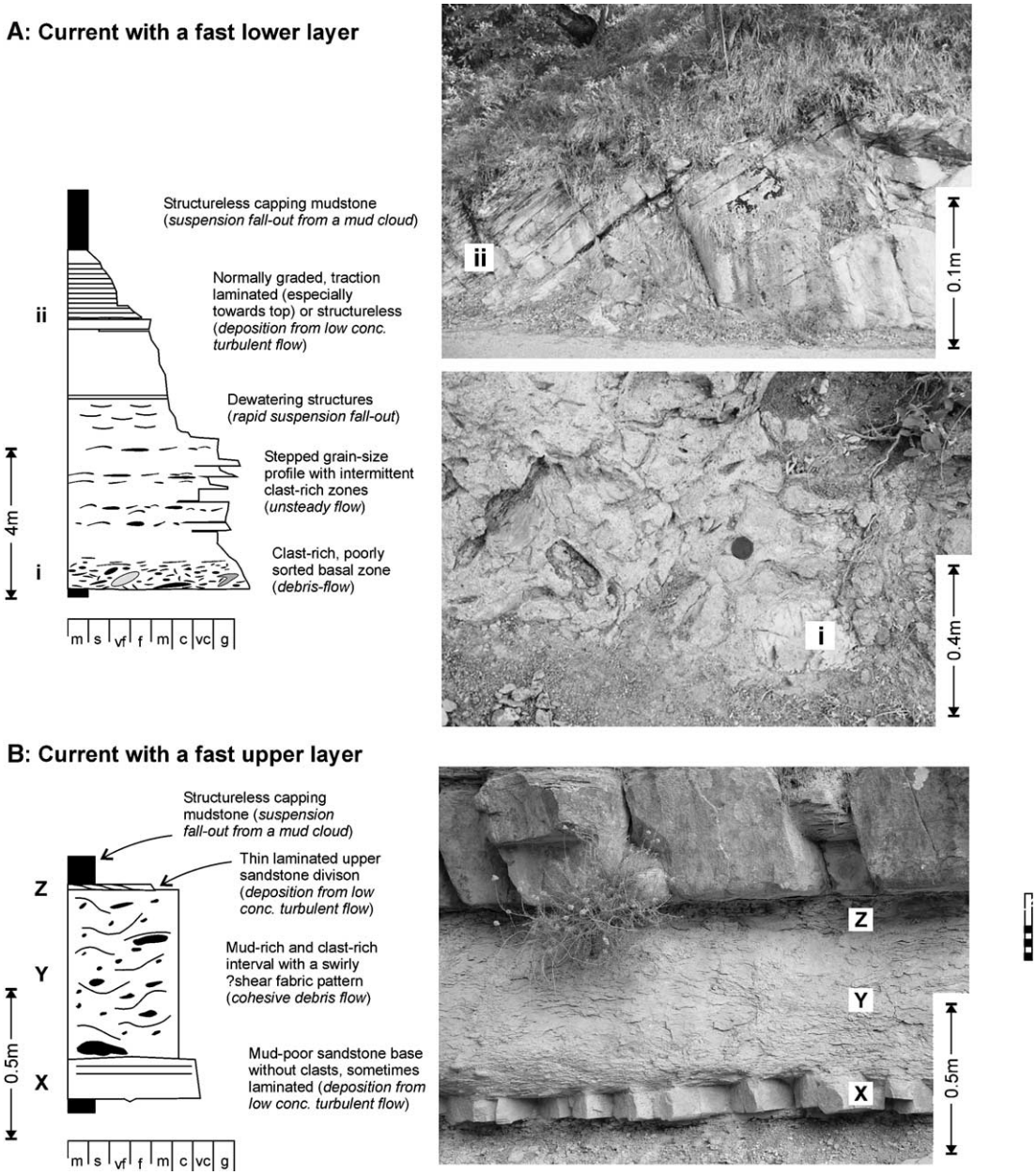

Fig. 14. Examples of beds preserved in ancient turbidite successions. (A) Sandstone bed from the Grès de Peïra Cava, Maritime Alps of SE France. This bed is interpreted as the deposit of a stratified sediment gravity flow with a faster-moving high-concentration lower region. (B) Sandstone bed with a tripartite bed structure from the Marnoso-arenacea, northern Apennines of Italy. This type of bed is interpreted to have been deposited by a stratified sediment gravity flow with a slower-moving, high-concentration, lower region. See text for further explanation.

single location the deposit will show a tripartite structure with the deposit of the high-concentration phase encased between the deposits of the relatively low-concentration flow phases (Fig. 11B). A significant proportion of sediment gravity flow deposits of the Miocene, Marnoso-arenacea Formation located in the Italian Apennines display this type of tripartite bed structure. These beds have been interpreted as debris flow deposits sandwiched between turbidites (Ricci Lucchi and Valmori, 1980; Talling et al., 2004; Amy et al., 2005—this issue) formed in an open basin-plain environment of the Apennine foredeep (Ricci Lucchi and Valmori, 1980; Argnani and Ricci Lucchi, 2001). The basal interval is composed of <20 cm, mud-poor (<15% in thin section; Talling et al., 2004), coarse- to fine-grained sandstone (Fig. 14B). The middle debrite sandstone interval is usually slightly finer and thicker (~20–90 cm) than the basal interval and relatively mud-rich (15–22% in thin section; Talling et al., 2004). It contains floating out-sized clasts several millimetres to tens of centimetres in diameter. The upper division is usually relatively thin (<20 cm), fine- to very fine-grained sandstone with millimetre-scale cross-lamination or parallel lamination.

Evidence that these deposits record a single flow event rather than several amalgamated event beds are (a) that the clast-rich debris flow units always occur within this tripartite vertical bed sequence and (b) long-distance correlations show that tripartite beds do not 'break-apart' into individual beds moving laterally (Talling et al., 2004; Amy et al., 2005—this issue). Correlations also show that the middle clast-rich interval pinches out rapidly (over <5 km) downstream (Talling et al., 2004). This geometry suggests that this portion of the bed was deposited en masse by a high-concentration flow. In comparison, the lower interval extends downstream of the pinch-out position of the middle interval (Talling et al., 2004). Beds with a similar tripartite vertical bed profile have been described from the Pennsylvanian Jackfork Group in Kansas (Hickson, 1999), Jurassic fans in the North Sea (Haughton et al., 2003), and the Miocene and lower Pliocene Laga Formation, Italy (Mutti et al., 1978), demonstrating that these bed types commonly occur in deep-water systems. Alternative explanations for the generation of these 'sandwich' beds are discussed by Haughton et al. (2003) and Talling et al. (2004).

6. Conclusions

The behaviour of stratified gravity currents was investigated using two-layer, laboratory flows composed of aqueous glycerol solutions. In a set of experiments the initial density and viscosity stratification was systematically changed in a manner that might occur in particle-laden currents with relatively low to high sediment concentrations. It has been shown previously that the vertical distribution of density and buoyancy profoundly affects the behaviour of laboratory currents (Gladstone et al., 2004). Results from this study show that the viscosity stratification also has an important effect on flow behaviour. In currents with relatively weak viscosity stratification the high-concentration basal layer is driven by inertia and propagates to the nose of the current, provided it has a larger buoyancy than the upper layer. On the other hand, in currents with relatively strong viscosity stratification the high-concentration lower layer is controlled by viscous forces and lags behind the flow front regardless of its relative buoyancy. These two flow types, with a relatively fast- and slow-moving lower layer, correspond to those with relatively high and low Reynolds numbers, respectively. We suggest that a transition in flow type occurs with the onset of transitional and laminar flow conditions because of enhanced drag at the lower flow boundary. In the present experiments this transition was observed at concentrations of between 70% and 80% glycerol for the lower layer.

The recorded temporal profiles of velocity and concentration of currents with relatively weak and strong viscosity stratification are different. Consequently, stratified currents carrying particles are likely to show different depositional histories and produce deposits with varied characteristics. The experimental results allow some speculation about the character of stratified flow deposits. Currents with a relatively fast-moving, high-concentration phase should deposit beds with high-concentration flow deposits overlain by those of more dilute flow. A current with a relatively slow moving, high-concentration phase should produce a bed with a tripartite structure with a high-concentration flow deposit sandwiched between the deposits of more dilute flow. Deposits with these bed structures are commonly observed in ancient turbidite successions. Experiments on strati-

fied flows using particles is suggested as a fruitful area of future work.

Acknowledgments

This research was funded by the United Kingdom Natural Environmental Research Council and Conoco (now ConocoPhilips) through the Ocean Margins LINK scheme (Grant number NER/T/S/2000/0106). Experiments were conducted in the University of Leeds, School of Earth Sciences, Fluid Dynamics Laboratory. Mark Franklin, Bob Bows, Gary Keech, David Forgerty (School of Chemistry), Phil Fields, Tony Windross are thanked for technical support and members of Sedimentology Group for assistance in running experiments. Jaco Baas, Suzanne Leclair and an anonymous reviewer helped to improve the original manuscript. Andy Hogg and Charlotte Gladstone provided useful discussion. Funding for the laboratory facilities used was provided by EPSRC (GR/R60843/01) and by a consortium of oil companies including BG, BHP, Chevron Texaco, Total, Exxon Mobil, ConocoPhillips, Amerada Hess and Shell. We also acknowledge the award of UK Natural Environment Research Council grant GR3/10015 that funded development of the UDVP system.

References

Allen, J.R, 1985. Principle of Physical Sedimentology. George Allen & Unwin, London. 272 pp.

Altinakar, M.S., Graf, W.H., Hopfinger, E.J., 1996. Flow structure in turbidity currents. Journal of Hydraulic Research 34, 713–718.

Amy, L.A., 2000. Architectural Analysis of a Sand-rich Confined Turbidite Basin; The Grès de Peïra Cava, South-East France. PhD Thesis, University of Leeds, UK.

Amy, L.A., McCaffrey, W.D., Kneller, B.C., 2004. The influence of a lateral basin-slope on the depositional patterns of natural and experimental turbidity currents. In: Joseph, P., Lomas, S.A. (Eds.), Deep-Water Sedimentation in the Alpine Basin of SE France: New Perspectives on the Grès d'Annot and Related Systems, Special Publication-Geological Society of London, vol. 221, pp. 311–330.

Amy, L.A., Talling, P.J., Peakall, J., Wynn, R.B., Arzola Thynne, R.G., 2005. Bed geometry used to test recognition criteria of turbidites and (sandy) debrites. Sedimentary Geology 179, 161–172 (this issue) doi:10.1016/j.sedgeo.2005.04.007.

Argnani, A., Ricci Lucchi, F., 2001. Tertiary silicoclastic turbidite systems of the Northern Apennines. In: Vai, G.B., Martini, I.P. (Eds.), The Apennines and Adjacent Mediterranean Basins. Kluwer Academic Press, pp. 327–350.

Arnott, R.W.C, Hand, B., 1989. Bedforms, primary structures and grain fabric in the presence of suspended sediment rain. Journal of Sedimentary Petrology 59, 1062–1069.

Barley, B., 1999. Deepwater problems around the world. Leading Edge 18, 488–494.

Barnes, H.A., 1989. Shear-thickening ("dilatancy") in suspensions of nonaggregating solid particles dispersed in Newtonian liquids. Journal of Rheology 33, 329–366.

Best, J.L., Kirkbride, A.D., Peakall, J., 2001. Mean flow and turbulence structure of sediment-laden gravity currents: new insights using ultrasonic Doppler velocity profiling. In: McCaffrey, W.D., Kneller, B.C., Peakall, J. (Eds.), Particulate Gravity Currents, Special Publication of the International Association of Sedimentologists, vol. 31, pp. 159–172.

Bouma, A.H., Normark, W.R., Barnes, N.E., 1985. Submarine Fans and Related Turbidite Systems. Springer Verlag, New York.

Branney, M.J., Kokelaar, P., 2002. Pyroclastic density currents and the sedimentation of ignimbrites. Geological Society Memoir, vol. 27. The Geological Society of London. 143 pp.

Buckee, C., Kneller, B., Peakall, J., 2001. Turbulence structure in steady, solute-driven gravity currents. In: McCaffrey, W.D., Kneller, B.C., Peakall, J. (Eds.), Particulate Gravity Currents, Special Publication of the International Association of Sedimentologists, vol. 31, pp. 173–187.

Chadwick, A., Morfett, J., 1992. Hydraulics in Civil and Environmental Engineering, 2nd edition Chapman and Hall.

Chen, Y.M., Pearlstein, A.J., 1987. Viscosity–temperature correlation for glycerol–water solutions. Industrial & Engineering Chemistry Research 26, 1670–1672.

Chikita, K., 1990. Sedimentation by river induced turbidity currents: field measurements and interpretation. Sedimentology 37, 891–905.

Choux, C.M.A., Baas, J.H., McCaffrey, W.D., Haughton, P.D.W., 2005. Comparison of spatial–temporal evolution of experimental particulate gravity flows at two different initial concentrations, based on velocity, grain size and density data. Sedimentary Geology 179, 49–69 (this issue) doi:10.1016/j.sedgeo.2005.04.010.

Coussot, P., 1997. Mudflow rheology and dynamics. Delft Hydraulics, International Association for Hydraulic Research.

De Wit, P.J., 1992. Rheological measurements on artificial muds. Report Number 9-92, Department of Civil Engineering., Delft University of Technology, Delft, Netherlands.

Felix, M., 2002. Flow structure of turbidity currents. Sedimentology 49, 397–419.

Ferreira, J.M., Diz, H.M., 1999. Effect of solids loading on slip-casting performance of silicon carbide slurries. Journal of the American Ceramic Society 82, 1993–2000.

Fisher, R.V., 1995. Decoupling of pyroclastic currents: hazards assessments. Journal of Volcanology and Geothermal Research 66, 257–263.

García, M.H., 1994. Depositional turbidity currents laden with poorly sorted sediment. Journal of Hydraulic Engineering 120, 1240–1263.

Ghibaudo, G., 1992. Subaqueous sediment gravity flow deposits: practical criteria for their field description and classification. Sedimentology 39, 423–454.

Gladstone, C., Ritchie, L.J., Sparks, R.S.J., Woods, A.W., 2004. An experimental investigation of stratified inertial gravity currents. Sedimentology 51, 767–789.

Hallworth, M.A., Huppert, H.E., 1988. Abrupt transitions in high-concentration, particle-driven gravity currents. Physics of Fluids 10, 1083–1087.

Hampton, M.A., 1972. The role of subaqueous debris flow in generating turbidity currents. Journal of Sedimentary Petrology 42, 775–793.

Haughton, D.W., Barker, S., McCaffrey, W.D., 2003. 'Linked' debrites in sand-rich turbidite systems — origin and significance. Sedimentology 50, 459–482.

Hickson, T.A., 1999. A study of deep-water deposition: constraints on the sedimentation mechanics of slurry flows and high-concentration turbidity currents, and the facies architecture of a conglomeratic channel overbank system. PhD Thesis, Stanford University, San Francisco.

Hilton, V.C., 1994. Architecture of Deep-Marine Confined Sandstone Bodies, Eocene–Oligocene Grès d'Annot Formation SE France. PhD Thesis, University of Leicester, UK.

Kneller, B.C., 1995. Beyond the turbidite paradigm: physical models for deposition of turbidites and their implications for reservoir prediction. In: Hartley, A.J., Prosser, C. (Eds.), Characterization of Deep Marine Clastic Systems. Special Publication, vol. 94. Geological Society of London, London, UK, pp. 31–49.

Kneller, B.C., Buckee, C., 2000. The structure and fluid mechanics of turbidity currents; a review of some recent studies and their geological implications. Sedimentology 47, 62–94.

Kneller, B.C., McCaffrey, W.D., 2003. The interpretation of vertical sequences in turbidite beds: the influence of longitudinal flow structure. Journal of Sedimentary Research 73, 706–713.

Kreiger, I.M., Dougherty, T.J., 1959. A mechanism for non-Newtonian flow in suspension of rigid spheres. Transactions of the Society of Rheology 3, 137–152.

Lide, D.L., Baysinger, G., Berger, L.I., Goldberg, R.N., Kehiaian, H.V., Kuchitsu, K., Lin, C.C., Rosenblatt, G., Smith, A.L., (Eds.), CRC Handbook of Chemistry and Physics, 84th Edition. Available online (http://www.hbcpnetbase.com/).

Liu, K.F., Mei, C.C., 1990. Approximate equations for the slow spreading of a thin sheet of Bingham plastic fluid. Physics of Fluids. A, Fluid Dynamics 2, 30–36.

Lowe, D.R., 1982. Sediment gravity flows: II. Depositional models with special reference to the deposits of high-concentration turbidity currents. Journal of Sedimentary Petrology 52, 279–297.

Major, J.J., Pierson, T.C., 1992. Debris flow rheology: experimental analysis of fine-grained slurries. Water Resources Research 28, 841–857.

Marr, J.G., Harff, P.A., Shanmugam, G., Parker, G., 2001. Experiments on subaqueous sandy gravity flows: the role of clay and water content in the flow dynamics and depositional structures. Geological Society of America Bulletin 113, 1377–1386.

McCaffrey, W.D., Kneller, B., 2001. Process controls on the development of stratigraphic trap potential on the margins of confined turbidite systems and aids to reservoir evaluation. American Association of Petroleum Geologists Bulletin 85, 971–988.

McCaffrey, W.D., Choux, C.M., Baas, J.H., Haughton, P.D.W., 2003. Spatio-temporal evolution of velocity structure, concentration and grain size stratification within experimental particulate gravity currents. Marine and Petroleum Geology 20, 851–860.

Middleton, G.V., 1966. Experiments on density and turbidity currents: II. Uniform flow of density currents. Canadian Journal of Earth Sciences 3, 627–637.

Middleton, G.V., 1993. Sediment deposition from turbidity currents. Annual Review of Earth and Planetary Sciences 21, 89–114.

Mohrig, D., Whipple, K.X., Midhat, H., Ellis, C., Parker, G., 1998. Hydroplaning of subaqueous debris flows. Geological Society of America Bulletin 110, 387–394.

Mulder, T., Alexander, T., 2001. The physical character of submarine density flows and their deposits. Sedimentology 48, 269–301.

Mutti, E., Nilsen, T.H., Ricci Lucchi, F., 1978. Outer fan depositional lobes of the Laga Formation (upper Miocene and lower Pliocene), east-central Italy. In: Stanley, D.J., Kelling, G. (Eds.), Sedimentation in Submarine Canyons, Fans and Trenches, pp. 210–223.

Normark, W.R., 1989. Observed parameters for turbidity–current flow in channel, reserve fan, Lake superior. Journal of Sedimentary Petrology 59, 423–431.

Peakall, J., McCaffrey, W.D., Kneller, B., 2000. A process model for the evolution, morphology, and architecture of sinuous submarine channels. Journal of Sedimentary Research 70, 434–448.

Peakall, J., Felix, M., McCaffrey, W.D., Kneller, B., 2001. Particulate gravity currents: perspectives. In: McCaffrey, W.D., Kneller, B.C., Peakall, J. (Eds.), Particulate Gravity Currents, Special Publication of the International Association of Sedimentologists, vol. 31, pp. 1–8.

Piper, D.J.W., Cochonat, P., Morrison, M.L., 1999. The sequence of events around the epicentre of the 1929 Grand Banks earthquake: initiation of debris flows and turbidity current inferred from sidescan sonar. Sedimentology 46, 79–97.

Postma, G., Nemec, W., Kleinspehn, K.L., 1988. Large floating clasts in turbidites: a mechanism for their emplacement. Sedimentary Geology 58, 47–61.

Ricci Lucchi, F., Valmori, E., 1980. Basin-wide turbidites in a Miocene, over-supplied deep-sea plain: a geometrical analysis. Sedimentology 27, 241–270.

Richardson, J.F., Zaki, W.N., 1954. Sedimentation and fluidisation: Part I. Transactions of the Institute of Chemical Engineers 32, 35–53.

Simpson, J.E., Britter, R.E, 1979. The dynamics of the head of a gravity current advancing over a horizontal surface. Journal of Fluid Mechanics 94, 477–495.

Stacey, M.W., Bowen, A.J., 1988. The vertical structure of turbidity current: theory and observation. Journal of Geophysical Research 93, 3528–3542.

Takeda, Y., 1991. Development of an ultrasound velocity profile monitor. Nuclear Engineering and Design 126, 277–284.

Talling, P.J., Amy, L.A., Wynn, R.B., Peakall, J., Robinson, M., 2004. Beds comprising debrite sandwiched within co-genetic

turbidite: origin and widespread occurrence in distal depositional environments. Sedimentology 51, 163–194.

van Kessel, T., Kranenburg, C., 1996. Gravity current of fluid mud on sloping bed. Journal of Hydraulic Engineering 122, 711–717.

Weimer, P., Link, M.H., 1991. Global petroleum occurrences in submarine fans and turbidite systems. In: Weimer, P., Link, M.H. (Eds.), Seismic Facies and Sedimentary Process of Submarine Fans and Turbidite Systems. Springer-Verlag, New York, pp. 9–67.

Wynn, R.B., Weaver, P.P.E., Masson, D.G., Stowe, D.A.V., 2002. Turbidite depositional architecture across three inter-connected deep-water basins on the Northwest African Margin. Sedimentology 49, 669–695.